PLOS PATHOGENS

RESEARCH ARTICLE

Caspase-mediated cleavage of murine norovirus NS1/2 potentiates apoptosis and is required for persistent infection of intestinal epithelial cells

Bridget A. Robinson[1], **Jacob A. Van Winkle**[1], **Broc T. McCune**[2], **A. Mack Peters**[1], **Timothy J. Nice**[1]*

1 Department of Molecular Microbiology and Immunology, Oregon Health and Science University, Portland, Oregon, United States of America, **2** Department of Microbiology, University of Texas Southwestern Medical Center, Dallas, TX, United States of America

* nice@ohsu.edu

OPEN ACCESS

Citation: Robinson BA, Van Winkle JA, McCune BT, Peters AM, Nice TJ (2019) Caspase-mediated cleavage of murine norovirus NS1/2 potentiates apoptosis and is required for persistent infection of intestinal epithelial cells. PLoS Pathog 15(7): e1007940. https://doi.org/10.1371/journal.ppat.1007940

Editor: Christiane E. Wobus, University of Michigan, USA, UNITED STATES

Received: March 26, 2019

Accepted: June 24, 2019

Published: July 22, 2019

Data Availability Statement: All relevant data are within the manuscript and its Supporting Information files.

Funding: This work was supported by NIH grant R01-AI130055 and by a faculty development award from the Sunlin and Priscilla Chou Foundation. The funders had no role in study design, data collection and analysis, decision to publish, or preparation of the manuscript.

Abstract

Human norovirus (HNoV) is the leading cause of acute gastroenteritis and is spread by fecal shedding that can often persist for weeks to months after the resolution of symptoms. Elimination of persistent viral reservoirs has the potential to prevent outbreaks. Similar to HNoV, murine norovirus (MNV) is spread by persistent shedding in the feces and provides a tractable model to study molecular mechanisms of enteric persistence. Previous studies have identified non-structural protein 1 (NS1) from the persistent MNV strain CR6 as critical for persistent infection in intestinal epithelial cells (IECs), but its mechanism of action remains unclear. We now find that the function of CR6 NS1 is regulated by apoptotic caspase cleavage. Following induction of apoptosis in infected cells, caspases cleave the precursor NS1/2 protein, and this cleavage is prevented by mutation of caspase target motifs. These mutations profoundly compromise CR6 infection of IECs and persistence in the intestine. Conversely, NS1/2 cleavage is not strictly required for acute replication in extra-intestinal tissues or in cultured myeloid cells, suggesting an IEC-centric role. Intriguingly, we find that caspase cleavage of CR6 NS1/2 reciprocally promotes caspase activity, potentiates cell death, and amplifies spread among cultured IEC monolayers. Together, these data indicate that the function of CR6 NS1 is regulated by apoptotic caspases, and suggest that apoptotic cell death enables epithelial spread and persistent shedding.

Author summary

Human Norovirus infection is highly contagious and the most common cause of acute gastroenteritis. Norovirus can be persistently shed after resolution of symptoms, perpetuating or initiating new outbreaks. Murine norovirus (MNV) is also persistently shed, enabling study of host and viral determinants of norovirus pathogenesis. We previously identified a critical role for MNV non-structural protein 1 (NS1), in persistence. Herein

Competing interests: The authors have declared that no competing interests exist.

we find that regulation of NS1 by host apoptotic caspases is required for infection of intestinal epithelial cells, but not for extra-intestinal spread. Additionally, we demonstrate that NS1 reciprocally promotes cell death and spread among epithelial cells. These data identify regulation of NS1 by host proteases and suggest that apoptotic death is a determinant of epithelial spread and persistence.

Introduction

Human norovirus (HNoV) is the most common cause of epidemic gastroenteritis worldwide, and can be particularly dangerous for infants and the elderly [1,2]. Viral shedding often persists asymptomatically for weeks to months after acute infection [3,4], and is a potential source for initiation of outbreaks. Despite recent success in development of *in vitro* systems to study HNoV infection [5,6], there remains a need for robust small animal models for investigating NoV biology. Murine norovirus (MNV) shares genotypic (ssRNA, positive-sense, ~7.5kb genome) and phenotypic (fecal-oral transmission, infection of intestinal epithelial cells (IECs), persistent shedding) features with HNoV. Therefore, studies of MNV have enabled considerable advances in understanding of norovirus biology [7–9].

All noroviruses express a non-structural polyprotein encoded by ORF1 and two structural capsid proteins (VP1 and VP2) encoded by ORFs 2 and 3, respectively [10–12] (Fig 1A). The non-structural polyprotein is cleaved by the internally-encoded viral protease into six 'mature' proteins (NS1/2, NS3, NS4, NS5, NS6, and NS7) [12–14]. Unlike related caliciviruses, NS1/2 of NoV remains intact for most of the virus life cycle and may be cleaved by host proteases rather than the viral protease [12,13]. NoV non-structural proteins associate with membranes and form the membranous viral replication complex [15–18]. Specific roles of NS5-7 have been defined as VpG cap, protease, and polymerase, respectively. However, the roles of NS1-4 are less well understood [19].

Our prior MNV studies compared acute strain CW3 (a plaque isolate of MNV-1) and persistent strain CR6 to identify viral determinants of pathogenesis and persistence [20–22]. We found that the capsid gene of CW3 ($VP1^{CW3}$) promotes extra-intestinal spread, whereas the NS1 gene of CR6 ($NS1^{CR6}$) promotes intestinal replication and persistent fecal shedding. An amino acid substitution at position 94 of CW3 NS1 (D94E) alters the conformation of a small structured region and can rescue CW3 persistence, suggesting the importance of this structured NS1 domain in persistence function [20,23]. Persistent and non-persistent strains similarly infect macrophages, dendritic cells, T-cells, and B-cells *in vitro* and *in vivo* [6,24,25], and utilize the same cell-surface receptor, CD300lf [26,27]. However, recent studies have shown that tropism for IECs *in vivo* requires $NS1^{CR6}$ in addition to CD300lf expression by non-hematopoietic cells [28,29]. Furthermore, only a minor lineage of IECs called tuft cells naturally express CD300lf and are susceptible to persistent infection by CR6 [28,30]. In contrast to the strain-dependent infection of IECs *in vivo*, CW3 and CR6 can replicate to similar titer in a cultured IEC cell line (M2C) that ectopically expresses CD300lf [29]. Thus, $NS1^{CR6}$ promotes IEC persistence *in vivo* via mechanisms other than receptor usage or replicative capacity *per se*.

In addition to viral determinants of MNV infection, critical aspects of the host anti-viral response have been identified. In particular, innate control of MNV replication is determined by the compartmentalized roles of type I (α/β) and type III (λ) interferon (IFN) [31]. Both types of IFN stimulate antiviral gene expression, but the IFN-α/β receptor (IFNAR) is expressed on most cell types, whereas the IFN-λ receptor (IFNLR) is preferentially expressed on epithelial cells [31]. Correspondingly, IFN-α/β is critical for control of MNV in myeloid

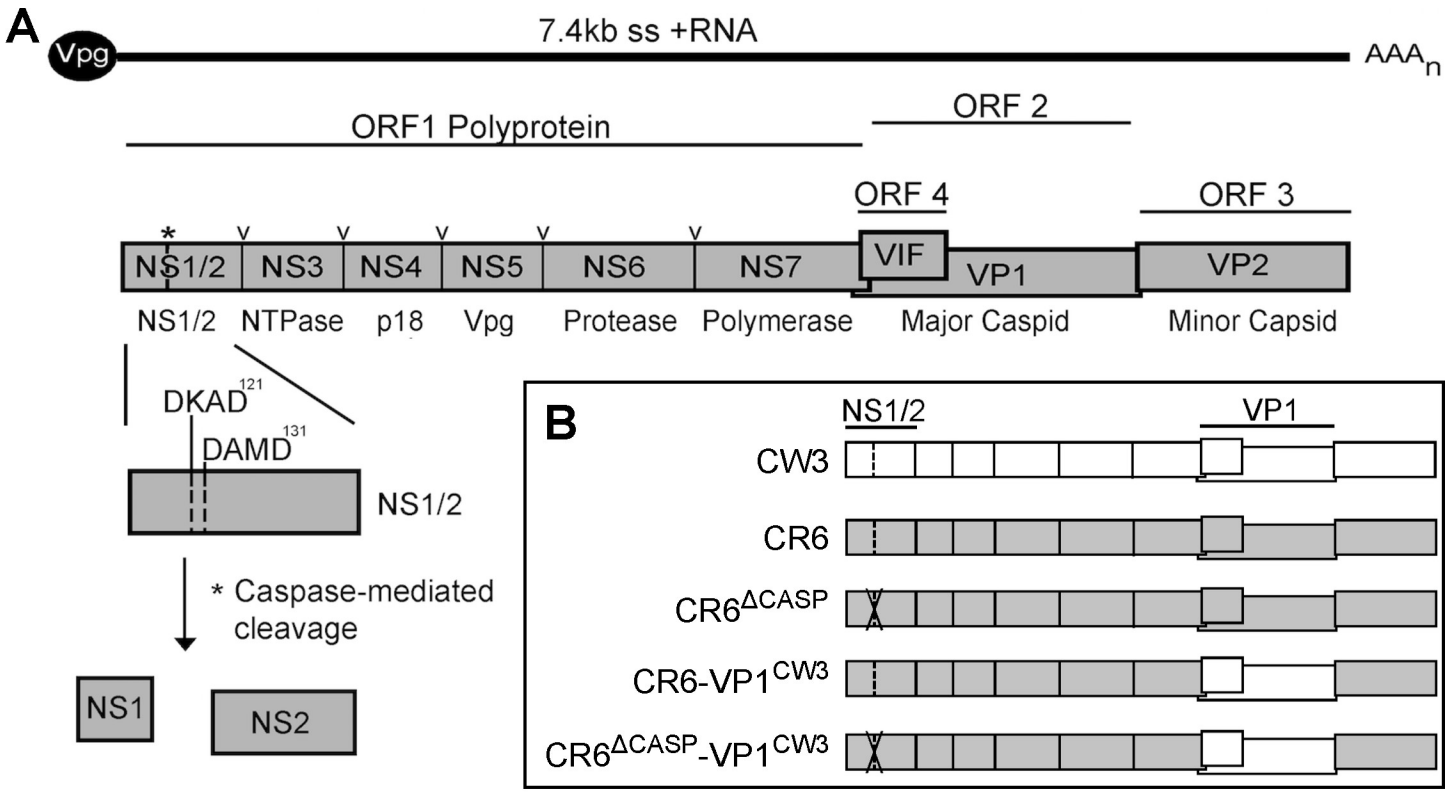
A
Vpg
7.4kb ss +RNA
AAAn
ORF1 Polyprotein
ORF 2
ORF 4
ORF 3
NS1/2
NS3
NS4
NS5
NS6
NS7
VIF
VP1
VP2
NS1/2
NTPase
p18
Vpg
Protease
Polymerase
Major Caspid
Minor Capsid
DKAD121
DAMD131
NS1/2
* Caspase-mediated cleavage
NS1
NS2
B
NS1/2
VP1
CW3
CR6
CR6ΔCASP
CR6-VP1CW3
CR6ΔCASP-VP1CW3

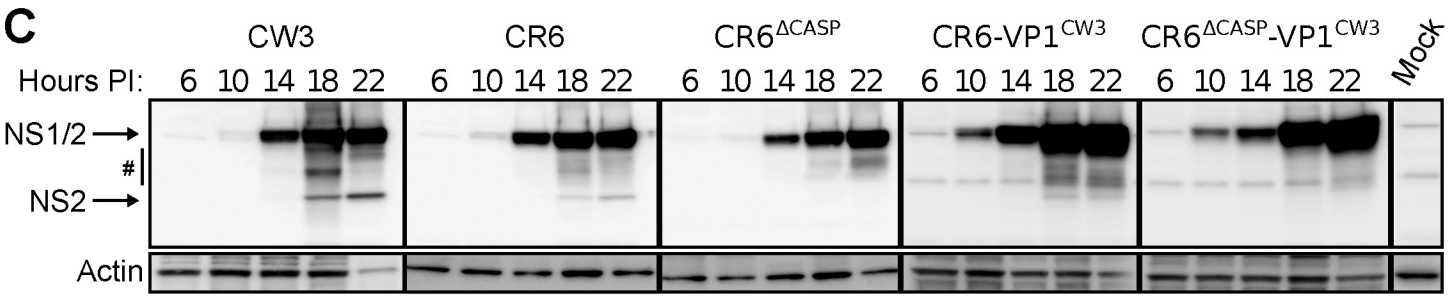
C
CW3
CR6
CR6ΔCASP
CR6-VP1CW3
CR6ΔCASP-VP1CW3
Mock
Hours PI: 6 10 14 18 22
NS1/2
#
NS2
Actin

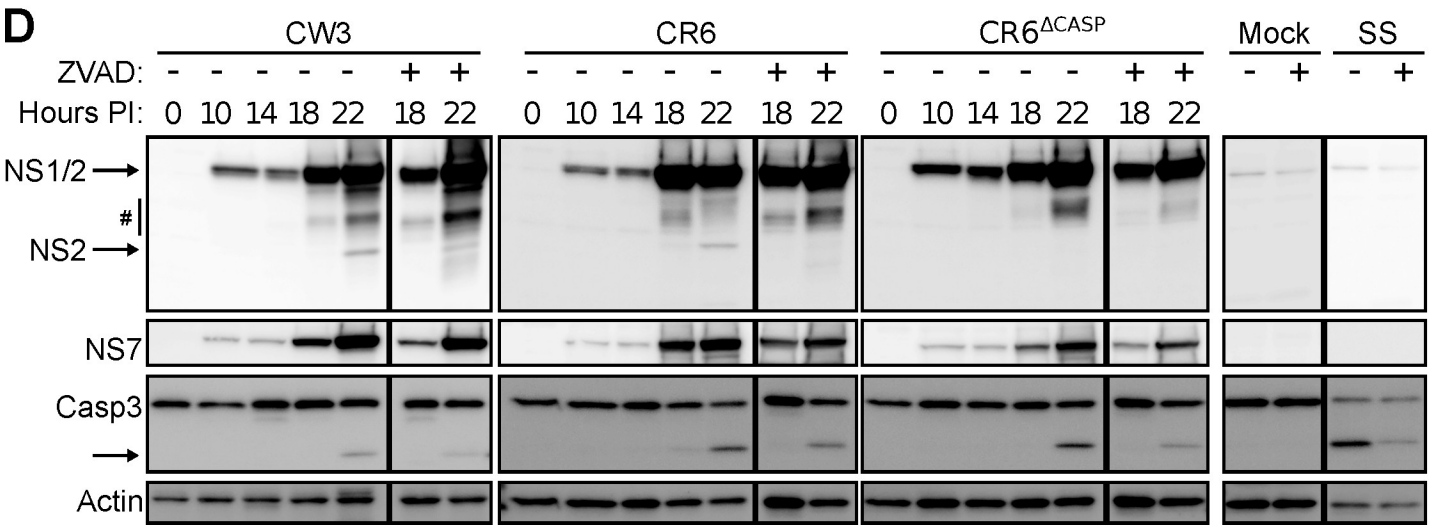
D
CW3
CR6
CR6ΔCASP
Mock
SS
ZVAD: - - - - - + +
Hours PI: 0 10 14 18 22 18 22
NS1/2
#
NS2
NS7
Casp3
Actin

Fig 1. MNV NS1/2 is cleaved by host caspases at late times-post-infection. (A) Schematic of MNV genomic organization, illustrating initial NS1/2 expression within the ORF1 polyprotein. Sites indicated in ORF1 are cleaved by the viral protease (**v**) and host caspases (*), the latter at aspartic acid residues 121 and 131 within two caspase motifs, $DKAD^{121}$ and $DAMD^{131}$. (B) Schematic representation of the five MNV clones used in these studies. D121G and D131G mutations are indicated by the X within NS1/2. (C) BV2 cells were infected with indicated strains of MNV (MOI = 1), and whole cell extracts (WCE) were analyzed via western blot (WB) at indicated times post-infection. Image is representative of 4 independent experiments. Arrows indicate full-length NS1/2 (45kD) and NS2 (28kD). Hash mark denotes background and caspase-independent bands >28kD. (D) BV2 cells were infected as in C, but subsequently treated with 50μM ZVAD-fmk at 10 hours post-infection, and WCE were probed for NS1/2, NS7, caspase 3, and actin via WB. Image is representative of 3 independent experiments. SS = staurosporine.

https://doi.org/10.1371/journal.ppat.1007940.g001

cells and prevents pathological dissemination [24,32,33], whereas IFN-λ is critical for control of MNV in IECs and prevents persistent shedding [34,35]. Deficiency of IFNLR promotes persistent infection, suggesting that $NS1^{CR6}$ counteracts the IFN-λ response [29]. However, CW3 persistence is not rescued in IFNLR-deficient mice [29,35] indicating that other host pathways are also important.

In addition to the IFN response, a general host response to many diverse viral genera is initiation of apoptosis. Correspondingly, viruses have evolved ways to hijack apoptotic machinery to their benefit. Apoptosis is a non-inflammatory, highly-regulated disassembly of the cell mediated by a family of cysteine proteases (caspases). Apoptotic cellular contents are packaged and released in membranous apoptotic bodies to be taken up by professional phagocytes and other neighboring cells [36]. Because apoptosis is an innate response to infection, many viruses have developed ways to delay induction of apoptosis such as expression of anti-apoptotic Bcl-2 family homologues [37,38]. In contrast, after virus production has reached its peak, many viruses actively promote apoptotic death or utilize 'apoptotic mimicry' to facilitate viral dissemination [38,39]. Additionally, some viruses rely on apoptotic caspases to cleave viral proteins as an additional level of regulation [40–42]. Thus, depending on its timing in relation to viral replication, apoptosis can be anti-viral or pro-viral and is therefore regulated by a diverse array of viral mechanisms.

HNoV and MNV infection both induce apoptosis, as indicated by association with markers of apoptosis in infected intestinal tissue [43–45]. Thus, these viruses have likely also developed mechanisms to regulate apoptosis in a pro-viral manner. Apoptosis has been most extensively studied in MNV-infected myeloid cells and is associated with down-regulation of anti-apoptotic survivin protein and activation of caspases 3, 7, and 9 [46,47]. Expression of the MNV ORF1 polyprotein is sufficient to induce apoptosis [48], indicating that one or more non-structural proteins are pro-apoptotic in the absence of viral replication. Additionally, NS1/2 encodes caspase cleavage motifs that are targeted by recombinant caspase 3 in a cell-free assay and separate NS1 from membrane-associated NS2 [12]. Thus, apoptosis during MNV infection may be facilitated by non-structural proteins and host caspases may reciprocally regulate NS1/2 function [20].

Herein, we identify a critical role for $NS1/2^{CR6}$ cleavage in MNV infection of the intestine and persistence. *In vitro*, we demonstrate that a minority of total NS1/2 protein is cleaved in a caspase-dependent manner, concurrent with the induction of apoptosis. Despite the relatively low proportion of total NS1/2 that is cleaved, $NS1/2^{CR6}$ cleavage is absolutely required for early infection in IECs and persistent shedding, independent of IFN-λ. Moreover, the cleavage of $NS1/2^{CR6}$ promotes apoptotic death of infected myeloid cells and spread among cultured IECs. These data suggest that controlled induction of apoptosis during viral egress promotes spread among IECs and is required for establishment of infection in IECs, the cellular reservoir of persistence.

Results

Host caspases cleave NS1/2 at late times post-infection

Previous cell-free studies identified two functional caspase motifs ($DKAD^{121}$ and $DAMD^{131}$) within NS1/2 that are cleaved by host caspase 3 [12] (Fig 1A), however, the targeting of these

sites during infection and functional consequences of NS1/2 cleavage was unknown. To test their role in persistent infection, we mutated these sites (D121G and D131G) within MNV strain, CR6 (CR6$^{\Delta casp}$, Fig 1B). In parallel, we generated a variant of CR6$^{\Delta casp}$ with the capsid of the systemic strain CW3 (CR6$^{\Delta casp}$-VP1^{CW3}) to enable determination of a role for NS1/2 cleavage in extra-intestinal tissues (Fig 1B) [20,49]. Analysis of NS1/2 protein expression following infection of BV2 myeloid cells revealed a similar level of full length NS1/2 production for all strains. However, infection with CW3, CR6, or the CR6-VP1^{CW3} chimera but not NS1/2 cleavage mutant strains resulted in a ~28 kDa NS2 fragment detectable at 18–22 hours post-infection (Fig 1C). The ~18kDa NS1 protein was inconsistently detected in cell lysates for any strain and may reflect the small overall proportion of cleaved NS1/2 or the accumulation of cleaved NS1 in the supernatant reported in a concurrent study [50]. Several fragments larger than 28 kDa (marked by #) were also observed, but were not dependent on caspase cleavage sites (Fig 1C) and may be generated by other proteases activated during cell death. Overall, these data show that cleavage of NS1/2 occurs during infection, depends on caspase motifs, and is independent of other genetic variation between CW3 and CR6.

To determine the temporal relationship between caspase activity and NS1/2 cleavage, we detected cleaved caspase 3 (active form) by western blot. Cleaved caspase 3 was observed at 18–22 hours post-infection for all strains tested, concurrent with NS1/2 cleavage (Fig 1D). To test the requirement of caspase activity for NS1/2 cleavage, we treated infected cells with the pan-caspase inhibitor, ZVAD-fmk. Inhibitor treatment reduced the proportion of cleaved caspase 3 and NS2 in cells infected with CW3 or CR6 but did not reduce the abundance of NS1/2 fragments larger than 28 kDa (Fig 1D). Together, these data demonstrate that NS1/2 is cleaved 18–22 hours post infection with persistent or non-persistent MNV strains, concurrent with induction of apoptosis, in a caspase-dependent manner.

CR6 NS1/2 cleavage promotes apoptosis in myeloid cells

In the course of characterizing caspase cleavage, we observed that the timing and magnitude of caspase 3 cleavage differed between viral strains (Fig 1D). To further compare caspase activity triggered by MNV infection, we used densitometry to quantify percentage of cleaved caspase 3 and poly ADP-ribose polymerase (PARP), a known target of apoptotic caspases [51]. We observed three-fold more activated caspase 3 and 10–20% more cleaved PARP in cells 18 hours post-infection with CR6 compared to CR6$^{\Delta casp}$ or CW3 (Fig 2A–2C). There were no significant differences in MNV polymerase (NS7) detected at 18–22 hours, but a trend toward more NS7 at 10–14 hours post-infection with strain CR6 compared to CR6$^{\Delta casp}$ or CW3. These data suggested that differences in caspase 3 and PARP cleavage were not due to increased peak replication in CR6-infected cultures, but may be related to earlier differences in replication kinetics (Fig 2B). Together with data in Fig 1, these data suggest that cleavage of CR6 NS1/2 (but not CW3 NS1/2) potentiates caspase activity.

To test whether our panel of MNV strains differed in induction of apoptotic cell death, we quantified surface presentation of phosphatidylserine (PS, Annexin V staining) and permeability to the LIVE/DEAD viability dye by flow cytometry following infection of BV2 cells. We found that CR6 infection resulted in two-fold more apoptotic cells (Alive Annexin V+) than CW3 or CR6$^{\Delta casp}$ (Fig 2D–2E). In contrast to CR6, most CR6-VP1^{CW3} infected cells lost membrane integrity and were stained with the LIVE/DEAD dye in addition to Annexin V (Fig 2D–2F), which is consistent with our recent findings that VP1^{CW3} drives lytic cell death and inflammatory cytokine production [49]. Even so, cells infected with CR6-VP1^{CW3} had 30–50% more total Annexin V staining than cells infected with the corresponding mutant strain CR6$^{\Delta casp}$-VP1^{CW3}, indicating that CR6 NS1/2 cleavage promotes cell death in conjunction

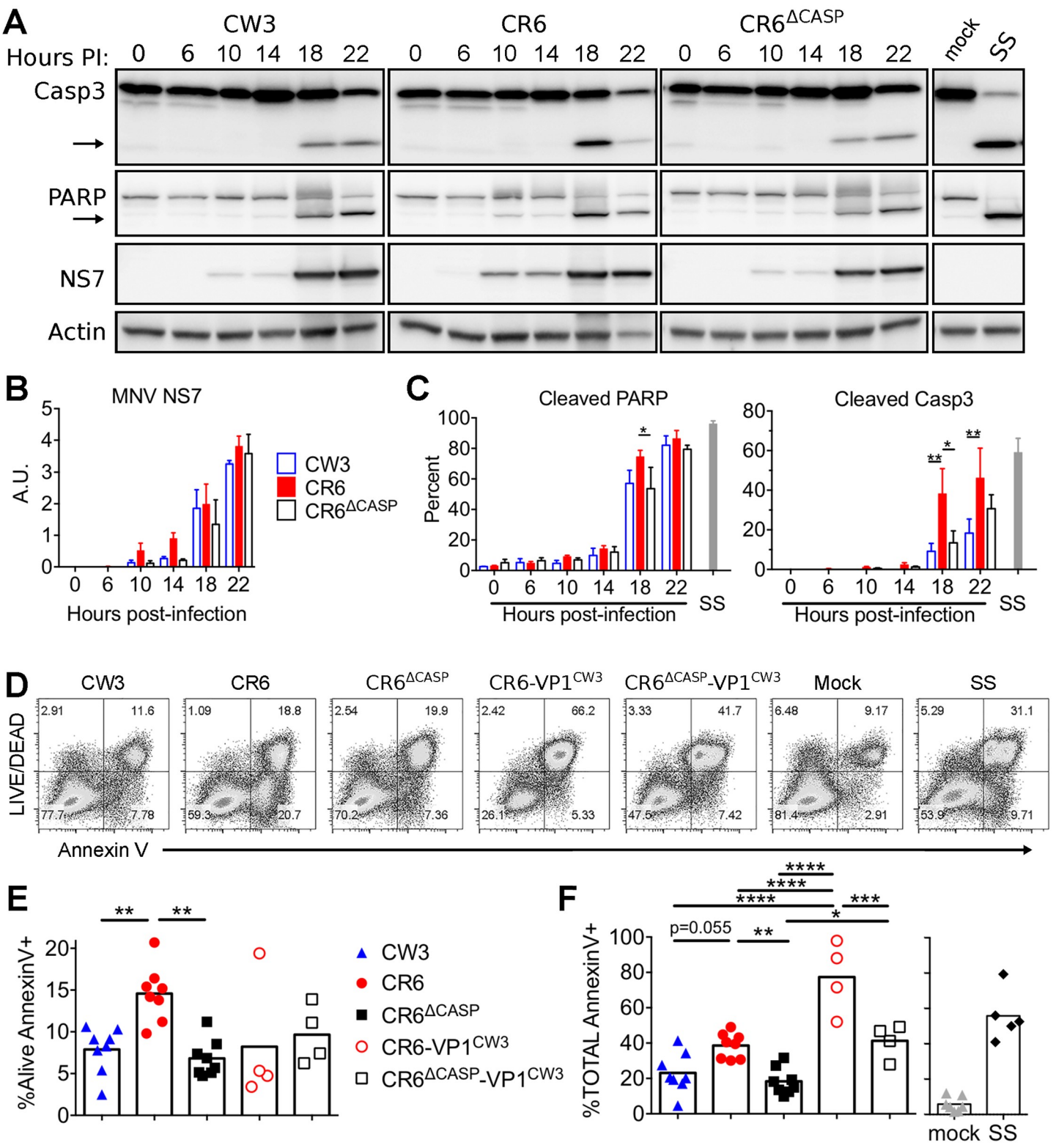

Fig 2. Cleavage of NS1/2 promotes apoptosis of myeloid cells. BV2 cells were infected (MOI = 1) with indicated MNV strains. (A-C) Whole cell extracts were collected at indicated times and analyzed via WB for caspase 3, PARP, actin, and MNV NS7. (A) Arrows denote cleaved fragments of caspase 3 and PARP. Images are representative of three independent experiments. (B) NS7 normalized to actin analyzed via densitometry. (C) Cleaved PARP and Caspase 3 were quantified as a proportion of total protein by densitometry. (D-F) Cells were harvested at 17 hours post-infection, stained with Annexin V and LIVE/DEAD viability stain, and analyzed via flow cytometry.

(D) Representative flow plots are shown from one of eight independent experiments. (E) Alive Annexin V+, and (F) total Annexin V+ cells from all experiments are graphed and mean values are indicated. Statistical significance was determined by one-way (E-F) or two-way (B-C) ANOVA, with Tukey's multiple comparison test. *, $p \leq 0.05$; **, $p \leq 0.01$; ***, $p \leq 0.001$; ****, $p \leq 0.0001$; SS, staurosporine.

https://doi.org/10.1371/journal.ppat.1007940.g002

with VP1^{CW3}-dependent lysis (Fig 2F). Together, these data suggest that CR6 NS1/2 cleavage by apoptotic caspases reciprocally promotes cleavage of caspase substrates and consequential cell death.

Cleavage of CR6 NS1/2 is not required for *in vitro* MNV replication in myeloid cells

The overall abundance of full-length NS1/2 and NS7 on western blots was similar between WT and mutant strains, indicating that viral protein production did not require NS1/2 cleavage (Figs 1C, 1D and 2A). However, many additional steps beyond protein production are required for assembly of infectious virus. So, we compared production of plaque forming units (PFU) over time from myeloid cells infected with our panel of MNV strains (Fig 1B) to assess whether production of infectious virus was dependent on CR6 NS1/2 cleavage. Mutation of NS1/2 cleavage sites did not significantly alter MNV replication kinetics or peak titers in BV2 cells following infection at a high multiplicity of infection (MOI, one PFU/cell) (Fig 3A). Following infection of BV2 cells at a low MOI (0.01 PFU/cell), there were modest differences in early 10–18 hour titer, but all strains reached similar peak titers by 36 hours post-infection (Fig 3A). The similar peak titers are consistent with our ability to obtain high titer viral stocks of NS1/2 cleavage mutants (generated by low MOI infection of BV2 cells) and indicate that NS1/2 cleavage is not required for MNV replication in these cells.

To test the requirement of NS1/2 cleavage for replication in primary myeloid cells, we generated bone-marrow dendritic cells (BMDCs) and infected them with our panel of MNV strains. Similar to BV2 cells, replication of CR6 in BMDCs was minimally impacted by mutation of NS1/2 cleavage sites (Fig 3B and 3C). However, CW3 and CR6-VP1^{CW3} reached higher peak titer in WT BMDCs compared to other strains tested, suggesting that VP1^{CW3} promotes BMDC replication. CR6$^{\Delta casp}$-VP1^{CW3} grew similarly to CR6 but grew to lower peak titers than CR6-VP1^{CW3} (Fig 3B), suggesting that NS1/2 caspase cleavage may have a VP1^{CW3}-dependent role in BMDCs, possibly related to the increase in lytic cell death observed for CR6-VP1^{CW3} (Fig 2D–2F, [49]). In parallel with WT BMDCs, we tested the role of STAT1-dependent IFN responses by comparing growth of our MNV strains in *Stat1*$^{-/-}$ BMDCs. All MNV strains reached higher peak titers in *Stat1*$^{-/-}$ BMDCs compared to WT BMDCs (compare Fig 3B and 3C), as expected from prior studies of STAT1-dependent immunity to MNV [24]. However, there were no statistically significant differences in growth that could be attributed to NS1/2 cleavage (Fig 3C). Overall, these data indicate that NS1/2 cleavage is not strictly required for replication of MNV in myeloid cells, but may promote BMDC replication in a VP1^{CW3}-dependent manner.

NS1/2 cleavage is not required for lethal systemic infection

Stat1$^{-/-}$ mice exhibit a profound inability to control systemic replication and succumb to infection in a VP1^{CW3}-dependent manner [20–22,32,33]. To test whether NS1/2 cleavage mutations impair this pathological MNV replication, we orally inoculated *Stat1*$^{-/-}$ mice with CR6-VP1^{CW3} or CR6$^{\Delta casp}$-VP1^{CW3} and monitored animals daily for signs of distress. Infection with CW3 or CR6-VP1^{CW3} resulted in 100% lethality with similar kinetics (Fig 4A). As expected, CR6-infected controls remained healthy due to lack of VP1^{CW3}-facilitated systemic spread

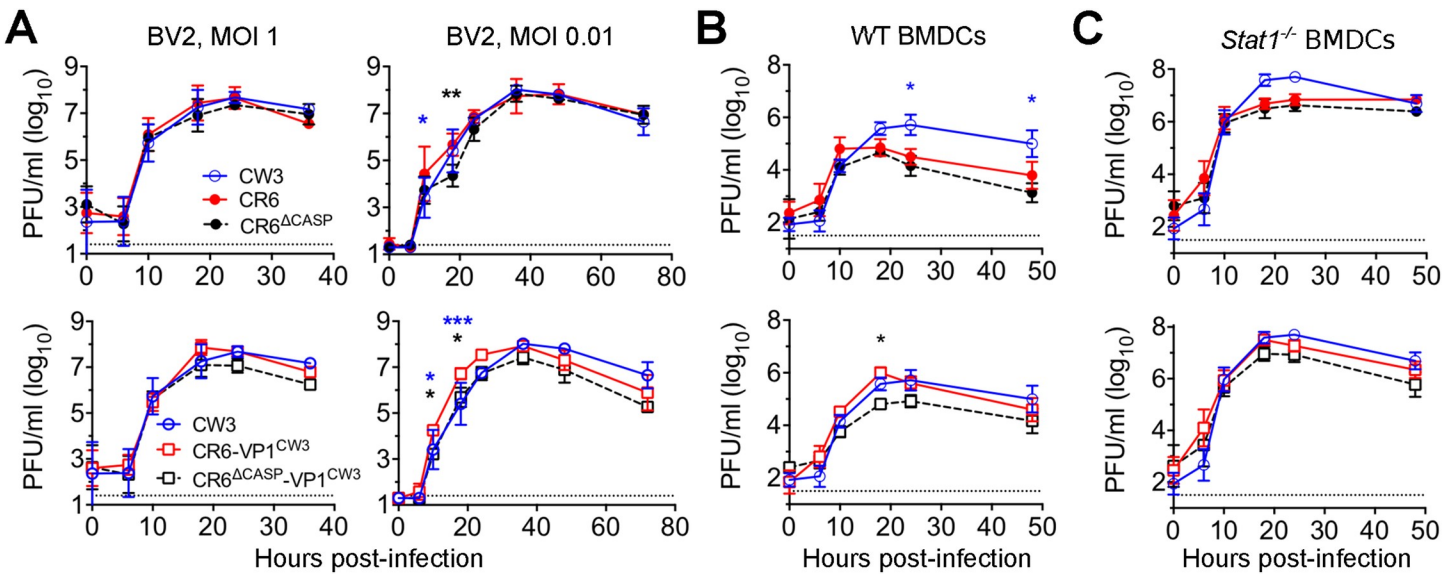

Fig 3. Cleavage of NS1/2 is not required for *in vitro* MNV replication in myeloid cells. BV2 cells (A), WT BMDCs (B), or *Stat1*$^{-/-}$ BMDCs (C) were infected with the indicated strain of MNV at MOI 0.01 (A) or MOI 1 (A-C) and infectious virus was analyzed at indicated times post-infection via plaque assay. Dotted lines indicate limit of detection. Error bars indicate SEM. Statistical significance was determined via two-way ANOVA with Tukey's multiple comparisons test. Significant differences shown are between CR6 (top) or CR6-VP1^{CW3} (bottom) and the strain indicated by the color of the asterisk. *, $p \leq 0.05$; **, $p \leq 0.01$. BMDCs = bone marrow-derived dendritic cells. Data are an average of at least three independent experiments.

https://doi.org/10.1371/journal.ppat.1007940.g003

[20]. These *in vivo* pathogenesis data suggest that NS1/2 cleavage is not required for lethal pathology resulting from uncontrolled, systemic infection of myeloid cells, consistent with no NS1/2 cleavage requirement for *in vitro* replication in myeloid cells.

CR6 NS1/2 cleavage is required for intestinal tropism and persistence

To directly quantify the effect of NS1/2 cleavage on acute replication and tissue tropism, we inoculated WT mice with CR6, CR6$^{\Delta casp}$, CR6-VP1^{CW3}, or CR6$^{\Delta casp}$-VP1^{CW3} and analyzed tissue and stool titers at three days post-infection (Fig 4B). As expected from our prior studies, CR6 and CR6-VP1^{CW3} were detected on day three in the mesenteric lymph node (MLN), ileum, and colon. We also detected infectious virus shed in the feces of mice infected with CR6 and CR6-VP1^{CW3}, consistent with replication in intestinal tissue. In contrast, in mice infected with NS1/2 cleavage mutant strains CR6$^{\Delta casp}$ or CR6$^{\Delta casp}$-VP1^{CW3}, infectious virus was rarely detected in intestinal tissues, or being shed in the feces. However, despite severely compromised replication in ileum (10-fold) and colon (1000-fold), splenic titers of CR6$^{\Delta casp}$-VP1^{CW3} were not significantly different from CR6-VP1^{CW3} (Fig 4B). This indicates that NS1/2 cleavage is not required for systemic spread, consistent with *Stat1*$^{-/-}$ lethality data (Fig 4A). Overall, these acute titer data demonstrate that caspase cleavage of NS1/2 is specifically required for promoting early infection of intestinal tissue, the eventual site of persistence.

Due to limited early detection of NS1/2 cleavage mutants in the intestinal tissues, we predicted that NS1/2 cleavage would be required for intestinal persistence. Indeed, most mice infected with CR6$^{\Delta casp}$ or CR6$^{\Delta casp}$-VP1^{CW3} had undetectable viral genomes in tissues at 21 days post-infection whereas CR6 and CR6-VP1^{CW3} were present in the ileum, colon, and stool (Fig 4C). Altogether, these findings support a role for CR6 NS1/2 cleavage in establishing early infection of the intestine and subsequent persistence.

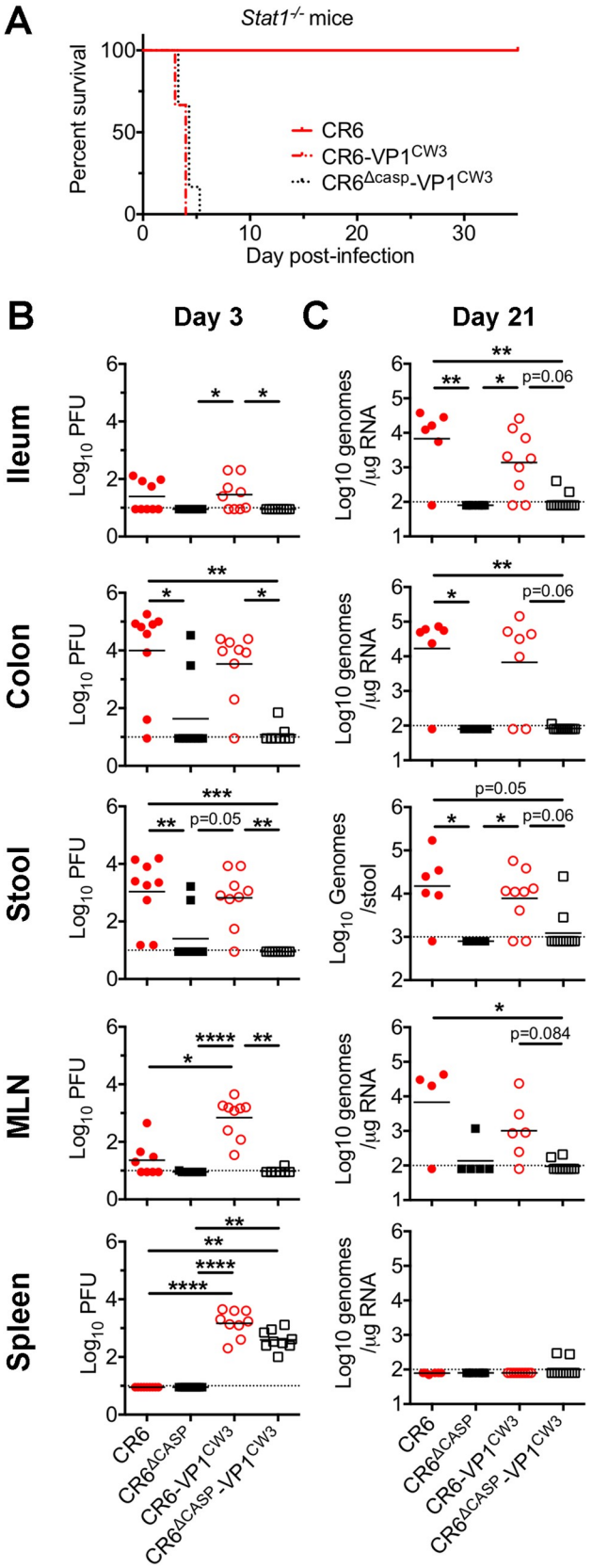

Fig 4. NS1/2 cleavage is required for intestinal tropism and persistence. (A) *Stat1*$^{-/-}$ mice were infected with the indicated strain and monitored daily for lethality. (B-C) WT mice were perorally infected with indicated viruses (1e6

PFU). At 3 (B) or 21 (C) days post-infection, tissues and stool were harvested and analyzed via plaque assay (B) or qPCR (D). Data are from 8–9 individual mice combined from 3 separate experiments, and mean values are indicated. Statistical significance was determined by Kruskal-Wallis test. *, $p \leq 0.05$; **, $p \leq 0.01$; ***, $p \leq 0.001$; ****, $p \leq 0.0001$; MLN, mesenteric lymph node.

https://doi.org/10.1371/journal.ppat.1007940.g004

CR6 NS1/2 cleavage is required for intestinal persistence independent of IFN-λ

IFN-λ plays a critical role in protection against persistent MNV infection of the intestine [35], so we sought to determine whether CR6$^{\Delta casp}$ persistence was restored in the absence of IFN-λ signaling. We infected WT or *Ifnlr1*$^{-/-}$ mice with CR6 or CR6$^{\Delta casp}$ and monitored shedding in the stool over time (Fig 5A and 5B), and persistence in the colon at 21 days post-infection (Fig 5C and 5D). Additionally, to determine whether an early barrier to MNV infection could be overcome with increased infectious dose, we included an experimental group inoculated with a 10-fold higher dose of CR6$^{\Delta casp}$ (1e7 PFU). MNV was shed in the stool of all WT mice infected with CR6 beginning on day three and continuing until the experimental endpoint, day 21. Consistent with the known role of IFN-λ, *Ifnlr1*$^{-/-}$ mice infected with CR6 shed greater than 10-fold more virus relative to WT mice (Fig 5A and 5B), and CR6 was detected in colon tissue at levels commensurate with fecal shedding (Fig 5C and 5D). In contrast, we were unable to detect shedding or colonic persistence of CR6$^{\Delta casp}$ at any time from WT or *Ifnlr1*$^{-/-}$ mice (Fig 5A and 5B). These data indicate that CR6 NS1/2 cleavage promotes persistent infection via a novel mechanism separate from IFN antagonism.

Cleavage of CR6 NS1/2 is critical for MNV infection of intestinal epithelial cells

Our preceding data demonstrated that disrupting CR6 NS1/2 cleavage prevented early infection of intestinal tissues and consequent persistent shedding in feces of either WT or *Ifnlr1*$^{-/-}$ mice (Figs 4 and 5). Because early infection of IECs is necessary for establishing persistent infection, we hypothesized that CR6 NS1/2 cleavage promoted early IEC tropism. To test this hypothesis, we infected WT or *Ifnlr1*$^{-/-}$ mice with our panel of MNV strains (Fig 1B) and quantified IEC infection at three days post-infection by flow cytometry. We pooled IECs isolated from proximal colon, cecum, and distal small intestine (devoid of Peyer's patches), and stained intracellularly for MNV NS1/2 (Fig 6A–6C). We rarely detected infected IECs in WT mice at this early timepoint, indicating that acute infection of IECs in our WT mice is below the limit of detection for this assay (Fig 6B). However, IEC infection was increased in *Ifnlr1*$^{-/-}$ mice relative to WT mice, indicating that IFN-λ limits early establishment of infection in the IEC reservoir (Fig 6A and 6C). CR6 and CR6-VP1^{CW3} were detected in an average of 40 IECs per million in *Ifnlr1*$^{-/-}$ mice, but we did not detect significant infection of IECs by NS1/2 cleavage mutants (Fig 6C). In parallel, to determine whether MNV strains that were not detected in IECs had otherwise initiated an infection, we quantified MNV in Peyer's patches by the more sensitive qPCR method. We detected viral RNA in Peyer's patches for the majority of CR6-infected mice, ~50% of CR6$^{\Delta casp}$-infected mice, and all mice infected with CR6-VP1^{CW3} or CR6$^{\Delta casp}$-VP1^{CW3} (Fig 6D and 6E). The CR6$^{\Delta casp}$-VP1^{CW3} genomes from Peyer's patches were examined by sanger sequencing and retained caspase cleavage mutations, which rules out reversion of these mutations as a prerequisite for robust Peyer's patch infection. The relationship between Peyer's patch replication for MNV strains in *Ifnlr1*$^{-/-}$ mice was similar to WT mice (Fig 6D and 6E), consistent with a minimal role of IFN-λ in non-epithelial cells within the Peyer's patches. These data indicate that the CR6-VP1^{CW3} strain, which robustly infects

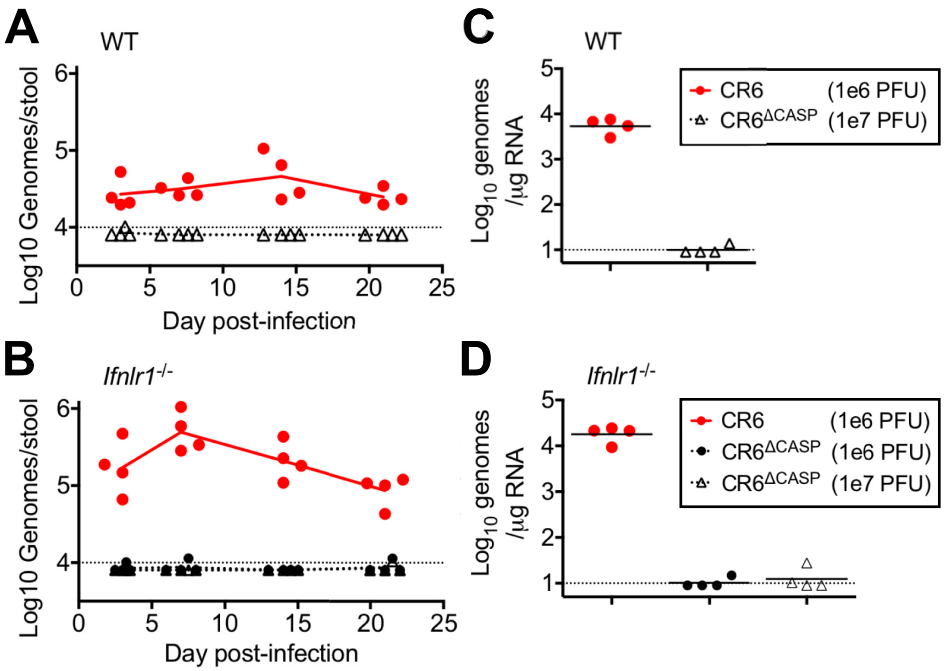

Fig 5. Caspase cleavage of NS1/2 is required independent of the IFN-λ response. WT (A, C) or *Ifnlr1*$^{-/-}$ (B, D) mice were infected by oral gavage with either 1e6 PFU or 1e7 PFU, as indicated. Fecal samples (A, B) were collected at 3, 7, 14, and 21 days post-infection, and colon tissue (C, D) was harvested at 21 days post-infection. All samples were analyzed via RT-qPCR, and the mean of each group (N = 4) is indicated. Dotted lines indicate limit of detection.

https://doi.org/10.1371/journal.ppat.1007940.g005

Peyer's patches, does not strictly require NS1/2 cleavage for initial infection of non-epithelial cells therein. Therefore, CR6 NS1/2 cleavage promotes early infection of IECs independent of the ability to initiate replication in Peyer's patches.

In complementary experiments, we infected mice with our panel of MNV strains and detected MNV genomes and EpCAM transcripts in small intestine sections via RNAscope at 48–72 hours post-infection (Fig 7). We included groups of WT and *Ifnar1 x Ifnlr1* double knockout (DKO) mice to compare IFN-restricted and unrestricted tropism, respectively. We reproducibly detected CR6 infection of IECs in WT mice at an average of one double positive (MNV and EpCAM) cell per cm of tissue length, whereas CR6-VP1^{CW3} was not consistently detected in IECs of WT mice and NS1/2 cleavage mutants were not detected at all (Fig 7A and 7B). In DKO mice, CR6 and CR6-VP1^{CW3} were detected with increased frequency relative to WT mice at seven and one DP cells per cm tissue length, respectively (Fig 7C and 7D). In contrast, infection of IECs by NS1/2 cleavage mutants remained below the limit of detection in DKO mice (Fig 7E). Infection of non-epithelial cells was observed inconsistently for all strains in WT mice and did not correlate with IEC infection; in DKO mice, CR6-VP1^{CW3} and CR6$^{\Delta casp}$-VP1^{CW3} robustly infected non-epithelial cells, whereas CR6 infection of non-epithelial cells remained inconsistent and CR6$^{\Delta casp}$ was not detected (Fig 7F). Taken together, these data demonstrate an IFN-independent role of CR6 NS1/2 cleavage in promoting early infection of IECs, the cellular reservoir of MNV persistence.

CR6 NS1/2 cleavage promotes spread among IEC monolayers

The infected IECs we observed *in vivo* on day three may be a result of viral amplification and spread rather than initial infection. To directly test the role of CR6 NS1/2 cleavage on initial

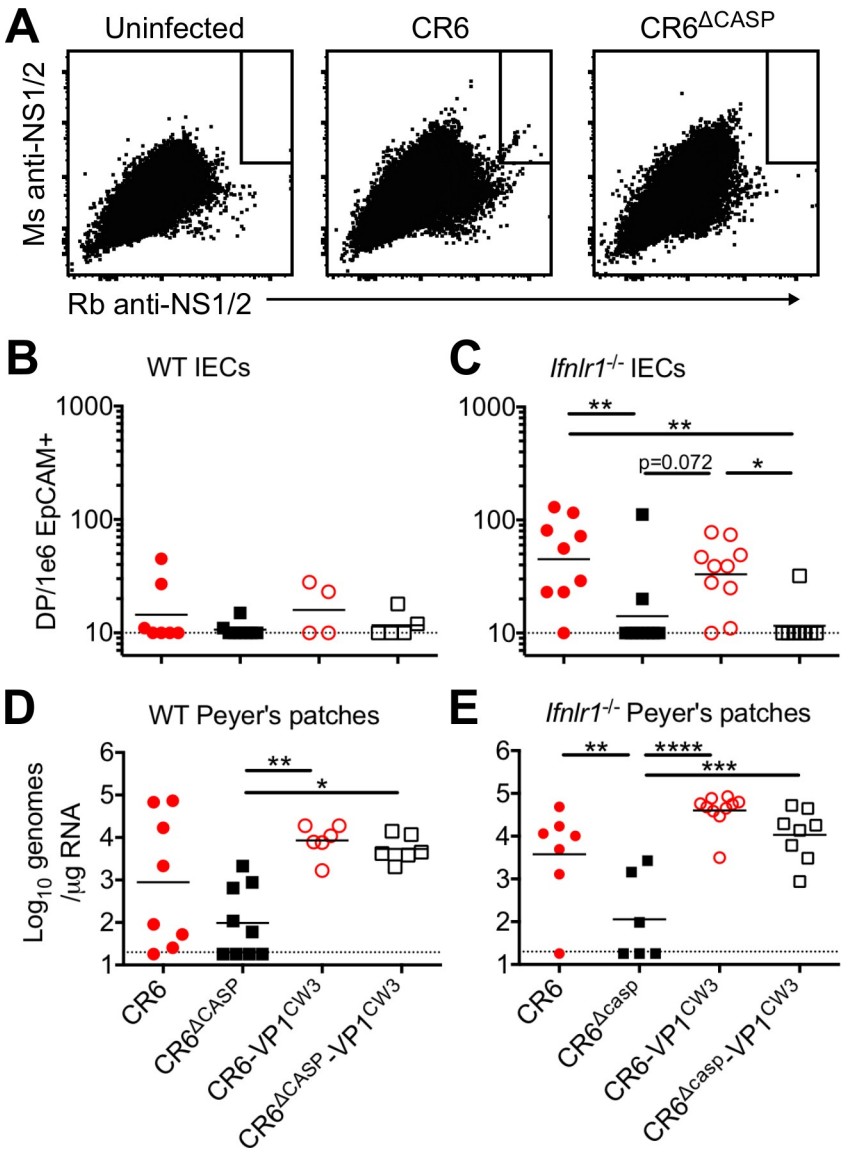

Fig 6. NS1/2 cleavage is necessary for infection of intestinal epithelial cells. Mice deficient for the IFN-λ receptor (A, C, E) or matched receptor-sufficient controls (B, D) were infected with indicated viruses and analyzed at three days post-infection. (A-C) Intestinal epithelial cells (CD45-, EpCAM+) were collected and doubly stained for NS1/2 as described in methods. (A) Flow plots representing concatenated data from five mice in C. Dotted line indicates limit of detection. (D-E) Peyer's patches were collected and analyzed via qPCR for MNV genomic RNA and normalized to RPS29. Data are combined from at least three separate experiments. Statistical significance determined by one-way ANOVA with Tukey's multiple comparisons test. *, $p \leq 0.05$; **, $p \leq 0.01$; ***, $p \leq 0.001$; ****, $p \leq 0.0001$.

https://doi.org/10.1371/journal.ppat.1007940.g006

infection of IECs, we used a previously characterized CD300lf-transduced IEC cell line (M2C-CD300lf, hereafter M2C), which can be infected by CW3 and CR6 [29]. We infected M2C cells with our panel of persistent and non-persistent strains (Fig 1B) and quantified replication over time by plaque assay (Fig 8A). Following infection at an MOI of one, persistent strains (CR6 and CR6-VP1^{CW3}) produced significantly more infectious progeny at 10 hours post-infection compared to non-persistent strains (CW3, CR6$^{\Delta casp}$, or CR6$^{\Delta casp}$-VP1^{CW3}). However, between 18–48 hours post-infection all strains reached similar peak titers with at

A

WT mice	Epithelial Infection	NON-Epithelial Infection
CR6	7/7	3/7
CR6$^{\Delta CASP}$	0/6	1/6
CR6-VP1^{CW3}	2/6	3/6
CR6$^{\Delta casp}$-VP1^{CW3}	0/5	2/5

B

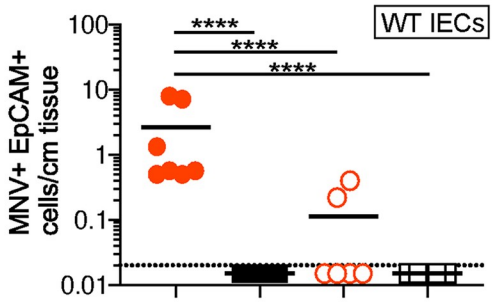

C

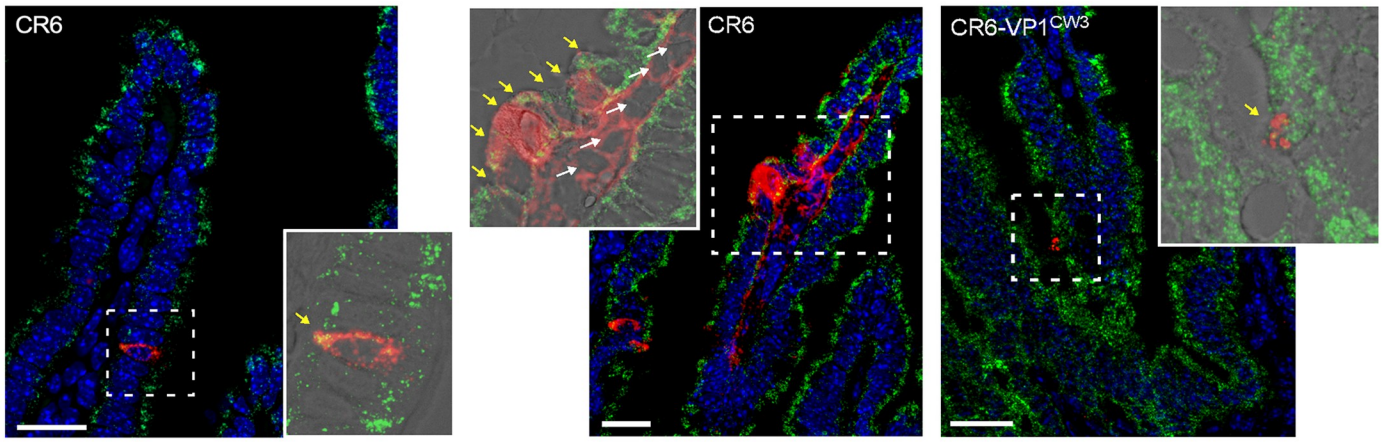

D

DKO mice	Epithelial Infection	NON-Epithelial Infection
CR6	4/4	2/4
CR6$^{\Delta CASP}$	0/3	0/3
CR6-VP1^{CW3}	7/7	7/7
CR6$^{\Delta casp}$-VP1^{CW3}	0/2	2/2

E

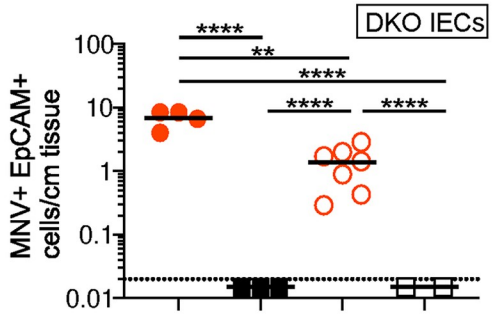

F

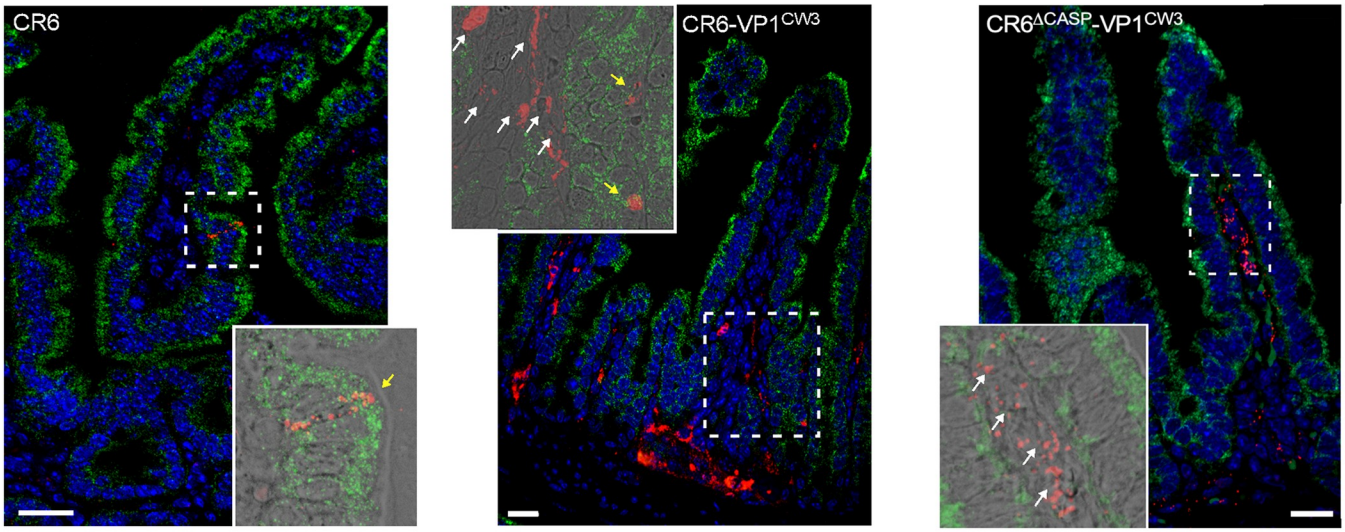

Fig 7. NS1/2 cleavage is necessary for infection of intestinal epithelial cells. Ileum tissue from MNV-infected WT (A-C) or DKO (D-F) mice was analyzed via RNAscope at 2–3 days post-infection. MNV RNA is in red, EpCAM is in green, and nuclei are stained with DAPI in blue. The tables in A and D indicate the total number of mice analyzed and the number of mice with MNV genome-positive cells in epithelial (EpCAM-positive) or non-epithelial (EpCAM-negative) compartments. Yellow arrows in images indicate MNV+ EpCAM+ cells and white arrows indicate MNV+ EpCAM-negative cells. Data points in B and E represent individual mice and indicate the number of MNV+ EpCAM+ cells per cm of tissue. White scale bar, 20μm. Statistical significance determined by one-way ANOVA with Tukey's multiple comparisons test. **, $p \leq 0.01$; ****, $p \leq 0.0001$.

https://doi.org/10.1371/journal.ppat.1007940.g007

most a two-fold difference between persistent and non-persistent strains (Fig 8A). Likewise, infection of M2C cells at a low MOI (0.01 PFU/cell) resulted in higher titers for persistent strains at 10 hours post-infection, but all strains reached similar titers by 18 hours post-infection (Fig 8B). However, between 24–72 hours following low-MOI infection, persistent strains proceeded to replicate robustly and reach similar peak titer as high MOI infection, whereas non-persistent strains replicated more slowly with 10-fold lower titer between 24–72 hours (Fig 8B). These findings differ from our earlier analysis in myeloid cells, where higher peak titers did not correlate with persistence phenotype (Fig 3), and suggest specific roles of CR6 NS1/2 cleavage in IEC infection.

To further characterize infection in IECs, we quantified infected cells by immunofluorescence staining for MNV NS7 following infection at MOI of one. Unexpectedly, only ~10% of M2C cells were NS7-positive between 14 and 24 hours post-infection, suggesting that MNV does not efficiently initiate replication in these cells. Strains CW3, CR6, or CR6$^{\Delta casp}$ all had a similarly low percentage of initially infected cells at 14 hours post-infection (Fig 8C and 8D). This equal infection suggests that early differences in titer at 10 hours (Fig 8A and 8B) are due to different rates of virus production per cell. Although the initial proportion of infected cells was similar between strains, the percentage of CR6-infected cells increased from 10 to 30% by 32 hours whereas the percentage of CW3 or CR6$^{\Delta casp}$ infected cells did not significantly increase (Fig 8C and 8D). Furthermore, visual inspection of CR6-infected M2C cell monolayers at 48–72 hours post-infection revealed patches of minimal cellularity whereas CW3 or CR6$^{\Delta casp}$ infected monolayers remained intact (Fig 8E). In sum, these data indicate that non-persistent strains are similarly able to initially infect IECs, but spread among IEC monolayers is facilitated by cleavage of CR6 NS1/2.

CR6 NS1/2 cleavage promotes death of IECs

We next sought to identify the cellular response altered by NS1/2 cleavage that may account for differential spread among IEC monolayers and establishment of IEC infection *in vivo*. Analyses in myeloid cells indicated that NS1/2 cleavage promoted apoptotic cell death (Fig 2). To test whether IEC apoptosis was also promoted by NS1/2 cleavage, we infected M2C monolayers with CW3, CR6, or CR6$^{\Delta casp}$ and characterized cleavage of NS1/2, caspase 3, and PARP by western blot. In contrast to the robust caspase 3 cleavage seen in infected BV2 cells, we detected less than 10% cleavage of caspase 3 in M2C lysates from infection with any strain at any timepoint and were infrequently able to detect NS1/2 cleavage at any time post-infection (Fig 9A). This reduced cleavage is consistent with the relatively low frequency of infected M2C cells and loss of cellularity in CR6-infected cultures (Fig 8C and 8E). Additionally, staurosporine treatment of M2C resulted in visible loss of cellularity, but less cleavage of caspase 3 (25% vs. 60%) and PARP (10% vs. 95%) compared to BV2 cells (Figs 9A–9E and 2A–2E). Despite the relatively low amount of caspase cleavage, M2C monolayers infected with CR6 had three-fold more caspase 3 and PARP cleavage than those infected with CW3 or CR6$^{\Delta casp}$ (Fig 9A–9C) with no significant difference in viral protein production (NS7, Fig 9A and 9B). To determine if differences in caspase activity of infected M2C cells correlated with a different proportion of apoptotic cells, we quantified Annexin V staining and cell lysis by flow cytometry. At

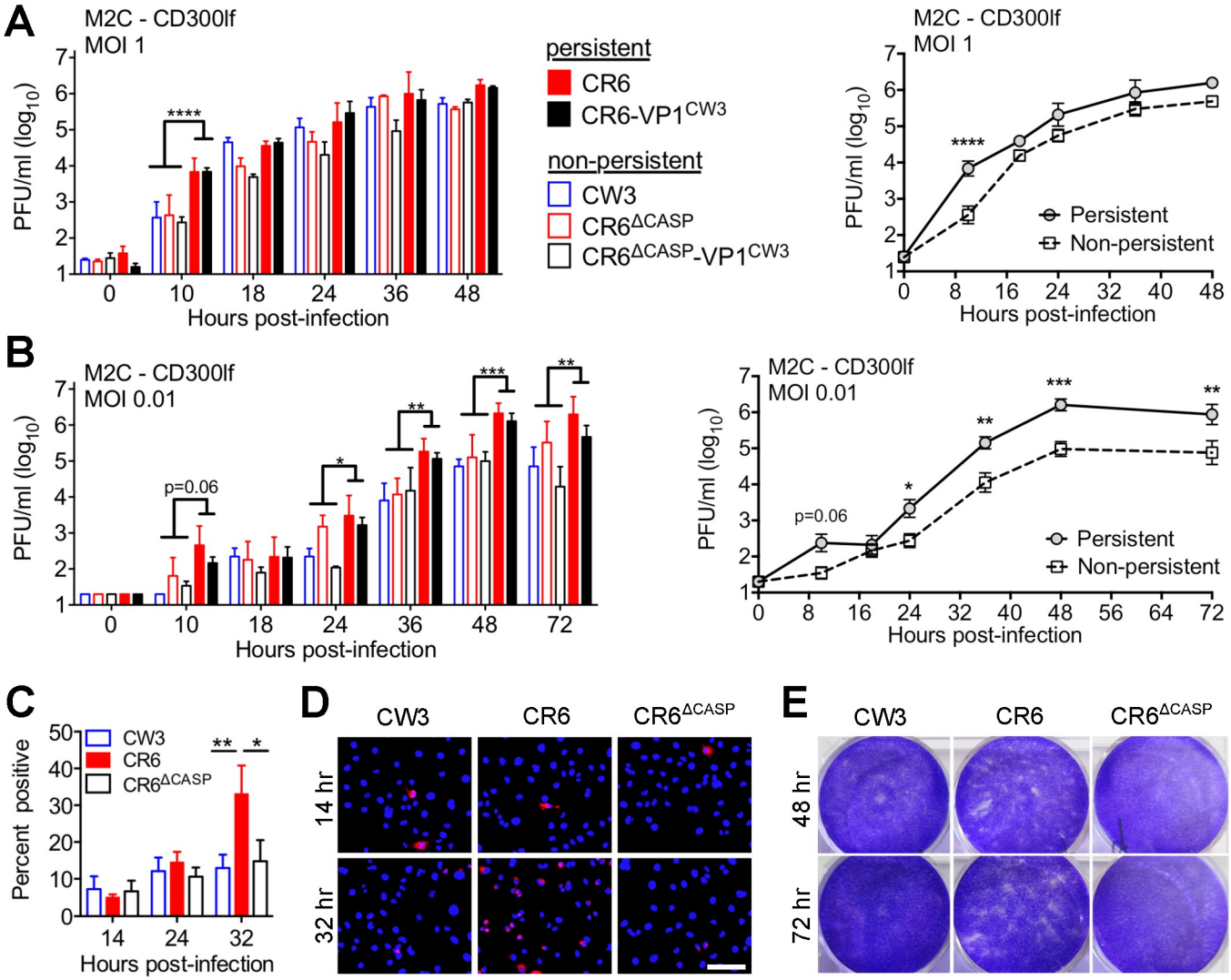

Fig 8. NS1/2 cleavage promotes spread among IEC monolayers. (A-B) M2C-CD300lf cells were infected with the indicated strains at MOI of 1 (A) or 0.01 (B) and production of infectious MNV was monitored over time by plaque assay on BV2 cells. Curves show growth of strains grouped by persistence phenotype. (C-E) M2C-CD300lf cells were infected with the indicated strains at MOI of 1 (C-D) or 0.1 (E) and stained for MNV NS7 immunofluorescence microscopy at the indicated time post-infection (C-D) or stained with crystal violet dye to visualize the cell monolayer (E). Data in A-C is grouped from at least three independent experiments. D and E are representative images, and white scale bar is 100μm. Statistical significance determined by two-way ANOVA of grouped data with Tukey's multiple comparison test. *, $p \leq 0.05$; **, $p \leq 0.01$; ***, $p \leq 0.001$; ****, $p \leq 0.0001$.

https://doi.org/10.1371/journal.ppat.1007940.g008

36 hours post-infection CR6 triggered a three-fold increase in apoptotic cells (Alive Annexin V+) whereas CW3 or CR6$^{\Delta casp}$ triggered only a two-fold increase over background (Fig 9D and 9E). Altogether, these data demonstrate that CR6 NS1/2 cleavage promotes apoptotic caspase activity and cell death of myeloid (BV2) and IEC (M2C) cell lines.

MNV-induced death occurred in a relatively low proportion of M2C cells over an extended time course with strain-dependent loss of cellularity (Fig 8E). To more comprehensively compare strain-dependent differences in this context, we used the incucyte imaging system to quantify confluency, Annexin V staining, and cytotox viability dye staining over time. Control M2C monolayers treated with staurosporine died rapidly with loss of confluency and increasing Annexin V and cytotox staining between 4–12 hours post-treatment (Fig 10). CR6 infected

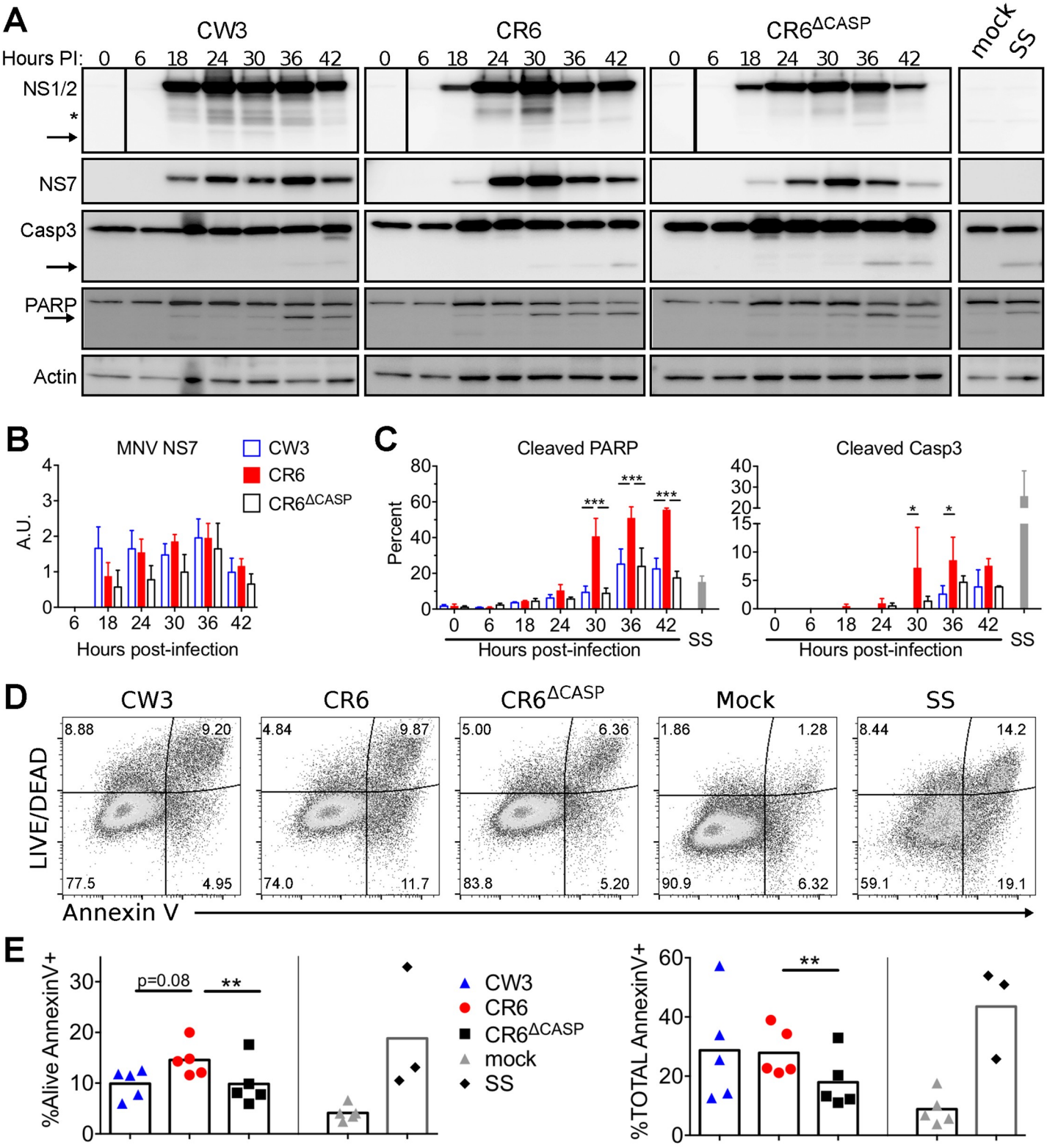

Fig 9. NS1/2 cleavage promotes death of IECs. M2C-CD300lf cells were infected (MOI = 1) with indicated MNV strains. (A-C) Whole cell extracts were collected at indicated times and analyzed via WB for MNV NS1/2, caspase 3, PARP, actin, and MNV NS7. (A) Arrows denote cleaved fragments of NS1/2, caspase 3 and PARP. Images are representative of three independent experiments. (B) NS7 normalized to actin analyzed via densitometry. (C) Cleaved PARP and Caspase 3 were quantitated as a proportion of total protein by densitometry. (D-E) Cells were harvested at 36 hours post-infection, stained with Annexin V and LIVE/DEAD viability stain, and analyzed

via flow cytometry. (D) Representative flow plots. (E) Alive Annexin V+, and total Annexin V+ cells are graphed and mean values are indicated. Data is from three to five independent experiments. Statistical significance was determined by one-way (E) or two-way (B-C) ANOVA with Tukey's multiple comparison test. *, $p \leq 0.05$; **, $p \leq 0.01$; ***, $p \leq 0.001$; SS, staurosporine.

https://doi.org/10.1371/journal.ppat.1007940.g009

monolayers also lost confluency over the course of the experiment whereas CW3 or CR6$^{\Delta casp}$ infected monolayers remained intact (Fig 10A). Monolayers infected with all MNV strains became positive for Annexin V and cytotox with similar kinetics, beginning at 12 hours post-infection and increased to a maximum at 48 hours (Fig 9A and 9B, S1–S5 Video). However, CR6 infection resulted in more overall Annexin V and cytotox staining over the course of the experiment than CW3 or CR6$^{\Delta casp}$ infection, as quantified by area-under-curve (AUC) analyses (Fig 9C). Prior to 24 hours post-infection, increased death of CR6-infected M2C cultures cannot be attributed to an increased proportion of infected cells (Figs 8C and 10A inset) but may be related to increased early virus production per cell (Fig 8A and 8B). At timepoints beyond 24 hours post-infection, the more effective spread of CR6 among these cultures (Fig 8C–8E) amplifies the magnitude of CR6-induced death. Although Annexin V positive M2C cells with intact membranes were detected by flow cytometry (Fig 9D and 9E), these live imaging data suggest that there is a rapid progression from apoptosis to lytic death in virally infected cells. Overall, these analyses of cell death suggest that CR6 NS1/2 cleavage promotes increased apoptotic and lytic death in IECs.

Caspase activity promotes spread among IEC monolayers

To determine whether caspase activity was required for the increased epithelial spread, we infected M2C-CD300lf monolayers with addition of caspase inhibitor ZVAD-fmk or vehicle control (DMSO) at 14 hours post-infection and quantified infected cells by immunofluorescence staining for MNV NS7. As seen in Fig 8, M2C cells infected with strains CW3, CR6, or CR6$^{\Delta casp}$ were similarly ~10% NS7-positive at 14 hours post-infection (Fig 11A). The proportion of CW3 or CR6$^{\Delta casp}$ NS7-positive cells did not increase over the 32-hour experiment, regardless of ZVAD treatment. However, CR6 NS7-positive cells increased to an average of 25% at 32 hours post-infection, and ZVAD treatment delayed this spread and resulted in significantly fewer NS7-positive cells at 24 hours post-infection (Fig 11A). Furthermore, visual inspection of CR6-infected M2C cell monolayers at 72 hours post-infection revealed a partial restoration of monolayer integrity when CR6-infected cells had been treated with ZVAD compared to when cells had been treated with DMSO control (Fig 11B and 11C). Therefore, caspase activity promotes spread among IEC monolayers. Taken together with our *in vivo* data, we propose that NS1/2 is a viral sensor of caspase activity whose cleavage promotes execution of cell death programs during viral egress, lateral spread among intestinal epithelial cells, and persistent shedding (Fig 11D).

Discussion

Herein, we demonstrate that caspase-mediated cleavage of the nonstructural protein, NS1/2, is critical for persistent MNV infection of the intestine. Importantly, we find that NS1/2 of non-persistent strain CW3 and persistent strain CR6 are similarly cleaved by caspases, suggesting that cleavage is required in conjunction with particular features unique to CR6 NS1, such as the conformational state of a previously characterized structured domain [23]. Our *in vitro* and *in vivo* analyses demonstrate that NS1/2 cleavage is not strictly required for viral replication in myeloid cells but is important for promoting infection in IECs, the cellular reservoir of persistence. Furthermore, our data indicate that CR6 NS1/2 cleavage potentiates apoptosis and

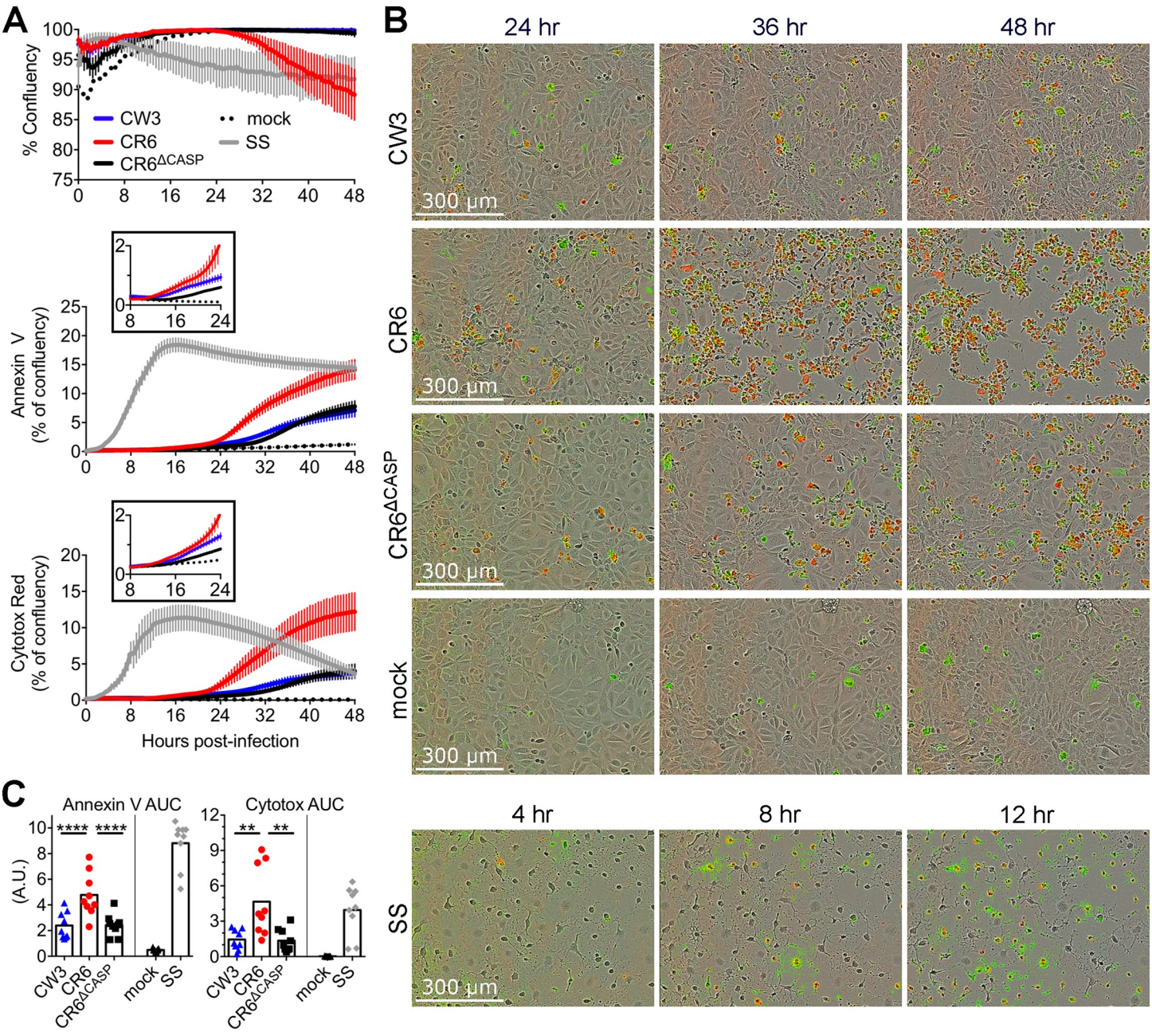

Fig 10. NS1/2 cleavage promotes death of IECs. M2C-CD300lf cells were infected (MOI = 1) with indicated MNV strains. Cells were imaged for 48 hours on the incucyte platform in the presence of Annexin V and cytotox red. (A) Quantitation of confluency, Annexin V area normalized to confluency, and cytotox red area normalized to confluency over time. (B) Representative images from indicated times post-infection. (C) Area under the curve was quantitated for data in A. Data points indicate individual wells. Data in A and C is combined from three independent experiments. Statistical significance in C determined by one-way ANOVA with Tukey's multiple comparison test. **, $p \leq 0.01$; ****, $p \leq 0.0001$; AUC, area under curve; SS, staurosporine.

https://doi.org/10.1371/journal.ppat.1007940.g010

lytic death, suggesting that regulation of cell death is a critical aspect of establishing early and consequential persistent infection of IECs.

NS1/2 was not previously known to play a role in cell death during MNV infection, but is required for viral replication beginning at the earliest stages of replication complex assembly. Norovirus replication occurs in the cytoplasm on cellular membranes with a variety of

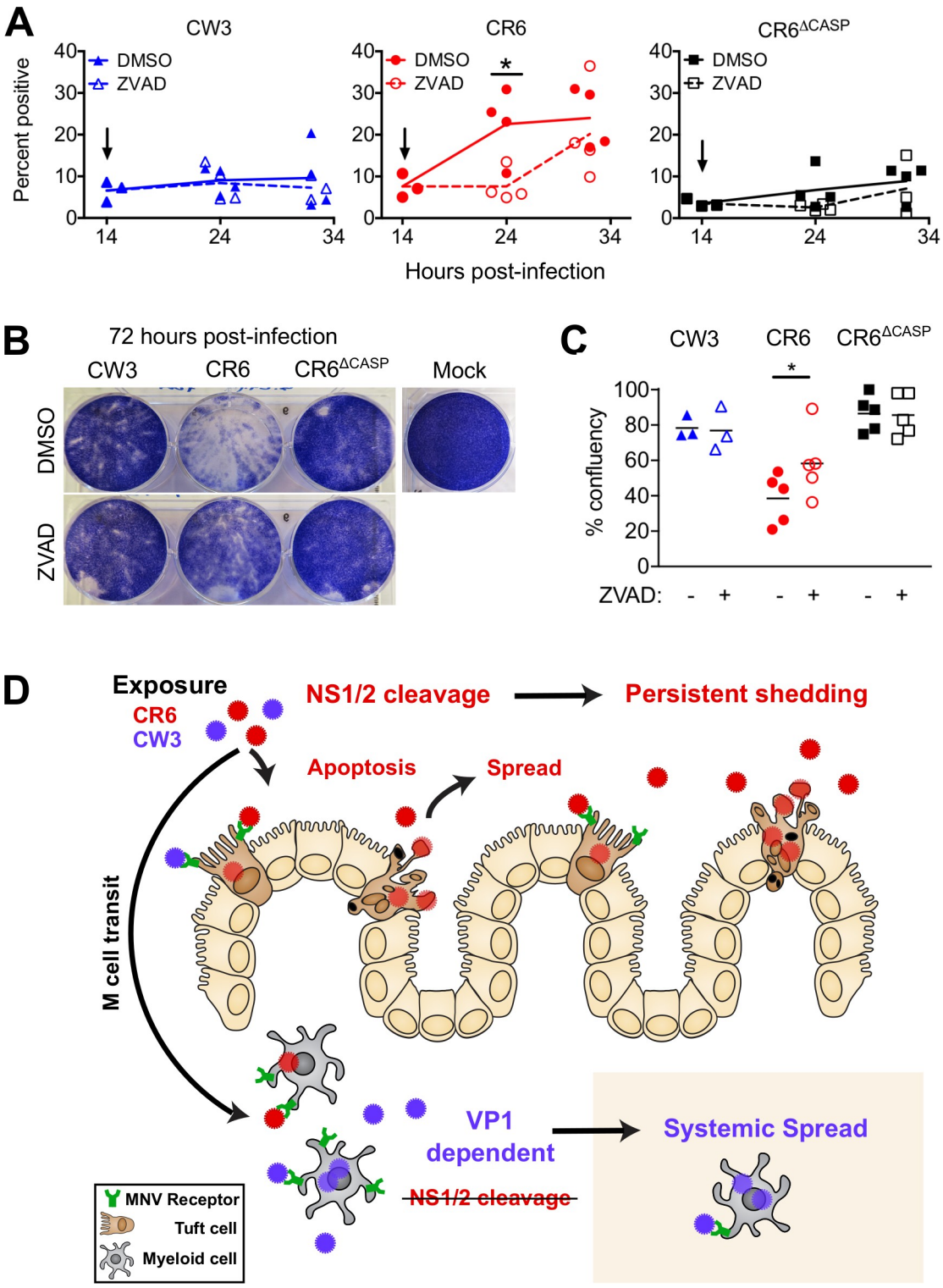

Fig 11. Caspase activity promotes spread among IEC monolayers. (A-C) M2C-CD300lf cells were infected with the indicated strains at MOI of 1 (A) or 0.1 (B-C) and DMSO or 50μM ZVAD-fmk as indicated were added at 14 hours post-infection. At the indicated times post-infection, cells were stained for MNV NS7 immunofluorescence microscopy (A) or stained with crystal violet dye to visualize the cell monolayer (B-C). Area of stained monolayers was quantitated by image analysis and normalized to mock infection (C). B is a representative image. Data in A and C is grouped from independent replicate experiments, with individual data points representing each replicate. Arrows in A indicate time of DMSO or ZVAD addition. Statistical significance determined by

two-way ANOVA of grouped data with Sidak's multiple comparison test. *, $p \leq 0.05$. (D) Model. MNV can cross the epithelial barrier via M cells and replicate in myeloid cells therein [25,69]. The capsid (VP1) of non-persistent strain CW3 (blue) promotes acute replication in intestinal myeloid cells and is required for spread to myeloid cells of systemic tissues. A different MNV gene, NS1 of persistent strain CR6 (red) is required for establishment of infection in rare CD300lf-expressing IECs (tuft cells), the eventual cellular reservoir of persistent intestinal infection and fecal shedding. Cleavage of CR6 NS1 from precursor NS1/2 promotes robust tuft cell infection by potentiating apoptotic caspase activity, death of infected tuft cells, and spread to dispersed target cells within the intestinal epithelium. In comparison to infection of IECs and intestinal persistence, NS1 and NS1/2 cleavage have relatively minimal impact on systemic replication.

https://doi.org/10.1371/journal.ppat.1007940.g011

organelle markers [15], and occurs near membranous vesicles [15,24]. MNV NS1/2 localizes to the endoplasmic reticulum (ER) [16,17] and promotes replication via membrane re-organization and through an interaction with the vesicle-associated membrane protein, VAPA [18,52]. Similarly, HNoV NS1/2 interacts with VAPA, localizes to vesicles, and disrupts vesicle trafficking when ectopically expressed [18]. Our data indicate that this early and essential role of NS1/2 remains intact when the caspase cleavage sites are mutated, and viral replication occurs normally in myeloid cells (Fig 2). NS1/2 cleavage only occurs after viral replication has peaked indicating that its role in promoting death, IEC infection, and persistence involves relatively late events in the viral life cycle.

The last step of the MNV replication cycle is egress, which occurs concurrently with induction of apoptosis. Therefore, NS1/2 cleavage and associated apoptotic death may be important for regulating release of viral progeny. How noroviruses are released from infected cells is not well understood, but infection of macrophages, DCs, or IECs does result in cell lysis ([24], Figs 2, 9 and 10) and non-enveloped viruses generally rely on cell lysis to release newly assembled virions. Apoptotic processes may alter egress by reducing lytic virion release and favoring retention of virions within cellular membranes. Indeed, a number of non-enveloped viruses utilize vesicle-associated egress as a means of evasion from immune detection, and vesicles with exposed phosphatidylserine allow for phagocytic uptake of novel target cells that may not express the viral receptor [53,54]. In addition to facilitating phagocytic uptake, membranes with PS can inhibit IFN responses via activation of Tyro3/Axl/Mer (TAM) receptor tyrosine kinases on target cells [55], which would allow more efficient viral replication. Thus, vesicular egress has the potential to dramatically change the outcome of infection via biophysical and immunological mechanisms. Intriguingly, recent studies by the Altan-Bonnet group indicate that MNV can be released from intact cells in PS-positive membranes [56] but the proportion of total virions released in this manner remains unknown. Therefore, it will be important in future work to consider the role of NS1/2 cleavage on regulation of this newly-described membranous egress and the role of viral association with membranes on spread among IECs.

The MNV receptor CD300lf is specifically expressed on MNV target cells, including myeloid cells and a specialized IEC subtype, tuft cells [26]. Tuft cells are a rare cell type in the intestinal epithelium and are dispersed among non-tuft, CD300lf-negative IECs [57]. Our analyses often found intestinal villi with multiple, adjacent epithelial cells infected (Fig 7C), raising the possibility of direct MNV spread to neighboring IECs, which could be mediated by cell death or apoptotic egress and regulated by NS1/2 cleavage. Our *in vitro* studies of infection in IEC monolayers support this hypothesis, and the dispersed nature of CD300lf-expressing tuft cells poses a strong selective pressure for efficient spread across receptor-negative stretches of the intestinal epithelium (Fig 11). Recent development of *in vitro* methods for differentiating tuft cells in primary IEC cultures [58] will enable future experiments to characterize spread in an IEC monolayer more representative of the *in vivo* scenario.

Regular turnover of the intestinal epithelium results in a short lifespan for differentiated epithelial cells, which undergo a specialized form of apoptotic cell death (anoikis) triggered as the cell detaches from the basal membrane and is shed into the lumen [59]. Specific Bcl-2

family proteins are critical players in anoikis [60,61], and display increased expression as IECs transit up the villus [61]. It is possible cleavage of NS1/2 (and perhaps NS1 directly) interferes with Bcl-2 family proteins as a means of altering the kinetics of the highly-regulated pathways that control apoptosis within differentiated IECs. Interestingly, similar to NS1/2 cleavage promoting apoptosis during infection, some Bcl-2 proteins (e.g. Bid) are also regulated via cleavage, in which the truncated version is the active, pro-apoptotic form of the protein [62]. An important future direction will be to examine whether NS1/2 interactions with the apoptotic machinery plays a role in maintaining IEC infection.

As mentioned above, PS receptor activation associated with apoptotic death could limit host responses. In contrast, virus production that results from cell lysis would promote inflammatory signals to alert the host of an infection. In addition to professional phagocytes, phagocytosis by non-professional phagocytes (e.g. epithelial cells) is critical for efficient clearance of apoptotic cells, and for limiting inflammation in tissues with high cellular turnover [63]. Specifically, in a mouse model of colonic injury, phagocytic uptake of apoptotic cells by IECs was sufficient for limiting inflammation in the colon [64], and phagocytosis mediated by epithelial cells is similarly critical for reducing inflammation in lung tissue [65] and mammary glands [66]. Thus, intestinal infection that promotes apoptotic death and the phagocytic uptake by IECs would limit host detection and provide a non-inflammatory environment that would allow more efficient infection of IECs and benefit MNV persistence.

Notably, we have not observed rescue of CR6$^{\Delta casp}$ MNV in animals deficient for the IFN-λ receptor, a key mediator of IEC antiviral responses (Fig 5). However, a concurrent study performed at Washington University has found that CR6$^{\Delta casp}$ can be rescued in IFNLR-deficient mice following high dose (10^7 PFU) inoculation [50]. Additionally, this study by Lee et al. shows that NS1 can be released from infected cells *in vitro* and immunization with NS1 is protective which strongly suggests an extracellular function [50]. The reason for a difference in IFNLR-dependency between these two studies remains unknown, but may be related to differences in MNV susceptibility between mouse vivaria. Specifically, persistently infected mice at Washington University shed one to two orders of magnitude more MNV genomes compared to mice at OHSU (Fig 5 in [50] compared to Fig 5 in this study), which may overcome the IFNLR-independent barrier to infection we have observed. These studies together raise the possibility that NS1/2 promotes infection of IECs through multiple non-redundant functions. There may be an IFNLR-antagonist function of the cell-free NS1 and a separate function within infected cells to promote apoptosis. Future work to identify molecular interactions with NS1/2 will be required to clarify the relationship between NS1/2 cleavage, IFNLR, NS1 secretion, and cell death. Our discovery of NS1/2 as an "apoptosis sensor" that reciprocally regulates apoptotic death and facilitates epithelial spread (Fig 11) has opened the door to such mechanistic studies and expanded our understanding of the requirements for viral persistence in the intestine.

Materials and methods

Ethics statement

All mice were maintained in specific-pathogen-free barrier facilities under animal protocols approved by the institutional animal care and use committee at Oregon Health & Science University (protocol # IP00000228) according to standards set forth in the Animal Welfare Act.

Cells, virus, and plaque assays

BV2 cells (gift from Herbert Virgin IV, Washington University, St. Louis, MO), a mouse microglial cell line [67], were maintained in DMEM (Life Technologies, ThermoFisher,

Carslbad, CA) with 5% fetal bovine serum (FBS) (VWR Seradigm, Radnor, PA), 1X Penicillin/Streptomycin/Glutamine (P/S/G) solution, and 10mM HEPES. M2C-CD300lf cells, a murine colonic epithelial cell line transduced with the MNV receptor, CD300lf [29], were maintained in DMEM with 10% FBS, 1X P/S/G, and 10mM HEPES. For bone-marrow derived dendritic cells (BMDCs), bone marrow was isolated from the long bones of each hind leg of either a WT or *Stat1*$^{-/-}$ mouse and suspended in RPMI (Life Technologies). Red blood cells were lysed using red blood cell lysis solution (Sigma, St Louis, MO) and remaining bone marrow cells were cultured in RPMI with 10% FBS, 1X P/S/G solution, 10mM HEPES, 1X Sodium Pyruvate, 1X non-essential amino acids, and 20ng/mL GM-CSF obtained from supernatants of GM-CSF-secreting cells (J558L, [68]). After seven days of culture (37C, 5% CO_2), non-adherent cells were collected, infected in suspension with indicated MNV strains (MOI = 1), and plated without GM-CSF for the indicated time. For indicated experiments, ZVAD-fmk (Cell Signaling Technology) was re-suspended in DMSO and added to cells at 70 μM. As a positive control for apoptosis assays, cells were treated with 1uM staurosporine (SS) (CST) for 3.5h, at 37C.

CR6$^{\Delta casp}$ MNV was generated using site directed mutagenesis as previously described [20] with the following primers: CR6 $D_{121}G$, 5'- GCCTAAGGAAGATAAAGCCG**G**TGCGCCC TCCCATGCG and CR6 $D_{131}G$, 5'-TGCGGAGGACGCCATGG**G**TGCAAGGGAGCCCA TAATTGG. The targeted residue is underlined with the mutation in bold. Correct mutations were verified via sanger sequence analysis.

MNV stocks were generated from plasmids, as described [22]. Briefly, plasmids encoding viral genomes of parental CW3 (Murine norovirus GV/MNV-1/2002/USA, clone CW3, GenBank accession no. EF014462.1), parental CR6 (Murine norovirus GV/CR6/2005/USA, GenBank accession no. JQ237823), CR6-VP1^{CW3} [20,22] and the two NS1/2$_{\Delta casp}$ viral genomes generated herein, were individually transfected into 293T cells (ATCC #CRL-3216). Forty-eight hours post-transfection, cells were frozen, thawed, vortexed, and spun at 3,000xg to remove large debris. Supernatants were expanded by two passages at MOI <0.05 in BV2 cells, and p2 virus supernatant was filtered (0.2 μm), concentrated by ultra-centrifugation through a 30% sucrose cushion, and titered via plaque assay.

Plaque assays were performed in BV2 cells, similar to previously described methods [20]. Briefly, BV2 cells were grown in 6well plates, infected with serial dilutions of each sample (500μl per well, 1h, RT, on a rocking platform), after which the inoculum was removed and cells were overlaid with 1% methylcellulose in complete DMEM. At two to three days post-overlay, cells were fixed and stained with 20% EtOH / 0.1% crystal violet.

Immunofluorescence analyses

M2C-CD300lf cells were grown on coverslips, fixed with 3.7% paraformaldehyde/PBS for 15 minutes at room temperature, and permeabilized in PBS with 0.1% triton X-100 and 3% normal goat serum for one hour at room temperature. MNV infection was observed by staining with anti-MNV ProPol (NS6/7) (a gift from Dr. Kim Green, NIH) followed by anti-Rabbit IgG-Alexa 647 (Molecular Probes). Nuclei were stained with DAPI. Coverslips were mounted on slides with Vectashield (Vector Laboratories, Burlingame, CA), and imaged using a Zeiss ApoTome2 on an Axio Imager, with a Zeiss AxioCam 506 (Zeiss, Jena, Germany).

Incucyte live-cell imaging and analysis

Cells were seeded in a 96-well plate, allowed to form a confluent monolayer (~18-24h), and subsequently infected with MNV or UV-inactivated MNV (MOI = 0.5). Mock-infected cells, and cells treated with 1μM staurosporine were used for negative and positive controls,

respectively. Apoptosis and cell permeabilization were assessed via addition of Incucyte Annexin V Green and Cytox Red reagents (EssenBioscience, Ann Arbor, MI), respectively, following manufacturer protocols. Phase contrast and fluorescent images were collected with a 10x objective using the IncuCyte Dual Dolor ZOOM (EssenBioscience) imaging system at 30minute intervals over a 72h time course, maintained at 37˚C and 5% CO_2. Images were analyzed using Incucyte 2016A software (EssenBioscience) after Top-Hat background subtraction, with a 20μm radius.

Mice, infections, and tissue collection

Stat1$^{-/-}$ (*Stat1*^{tm1Dlv}) mice were originally obtained from the Jackson Laboratories (stock #012606). *Ifnlr1*$^{-/-}$ (generated from *Ifnlr1*$^{tm1a(EUCOMM)Wtsi}$) and *Ifnar1*$^{-/-}$ (*Ifnar1*^{tm1Agt}) were originally obtained from Washington University in St. Louis. *Ifnlr1*$^{-/-}$ and *Ifnar1*$^{-/-}$ were bred to generate *Ifnlr1*$^{-/-}$/*Ifnar1*$^{-/-}$ mice (DKO) and *Ifnlr1*$^{+/-}$/*Ifnar1*$^{+/-}$ (Dhet). Dhet and DKO crossbreeding yielded littermate mice deficient in neither (Dhet), both (DKO), or a single (*Ifnlr1*$^{+/-}$/*Ifnar1*$^{-/-}$ or *Ifnlr1*$^{-/-}$/*Ifnar1*$^{+/-}$) IFN receptor gene(s); these littermates were used for experiments to control for variability between litters.

All mice (7-9weeks old) were perorally infected with 1e6 PFU in a 25μL volume administered by pipet, with the exception of experiments in Fig 5 where 1e6 or 1e7 PFU (as indicated in figure) was administered by oral gavage in a 100μL volume. An equal proportion of males and females were maintained among experimental groups to mitigate results due to any unidentified sex-dependent variables. Same-sex mice, infected with the same MNV strain, were often co-housed for acute infection analyses (less than three days), but singly-housed for extended experiments to prevent continued transmission between animals.

Tissue samples, or a single fecal pellet, were collected in 2ml cryovials with 1mm zirconia/silica beads (Biospec, Bartlesville, OK), frozen in a dry ice/EtOH bath and stored at -80C. For plaque assay or RT-qPCR analyses, either 1ml DMEM or 1ml RiboZol (VWR) was added, respectively, and tissues were homogenized via bead-beating (1min, RT) prior to continued analysis.

RNA, cDNA, and RT-qPCR

RNA from tissues was extracted via RiboZol (VWR) protocols, and RNA from cells was extracted with the ZR Viral RNA kit (Zymoresearch, Irvine, CA). DNA contamination was removed with Turbo DNase (ThermoFisher), and 1ug of RNA was used to generate cDNA with the ImpromII reverse transcriptase (Promega, Madison, WI). Quantitative PCR was performed using PerfeCTa qPCR FastMix II (QuantaBio, Beverly, MA), and the following oligo/probes were used for detection: MNV genomic RNA—Forward primer CACGCCACCGATC TGTTCTG, Reverse primer GCGCTGCGCCATCACTC, and Probe TGCGCTTTGGAACAA TGG; RPS29—Forward primer GCAAATACGGGCTGAACATG, Reverse primer GTCCAA CTTAATG AAGCCTATGTC, and Probe CCTTCGCGTACTGCCGGAAGC.

Cell Lysates and Western blot

BV2 cells were grown and infected in 12well plates (2 e5 cells/well). Cells were lifted with trypsin/0.25% EDTA (Gibco, ThermoFisher), washed with 1X cold PBS, resuspended in 100 μL NP40 lysis buffer (Alfo Aesar, Havervill, MA) with protease inhibitor cocktail (Sigma, St Louis, MO), incubated on ice (15min with intermittent mixing), cleared via centrifugation (1min, 4C, full-speed), and diluted 1:1 with 2x SDS loading buffer (0.125 M Tris [pH 6.8], 4% SDS, 20% glycerol, 0.004% bromophenol blue, 10% beta-mercaptoethanol). Lysates were run on Novex Tris-Glycine gels (ThermoFisher), transferred to 0.2 μm PVDF (BioRad, Hercules, CA), blocked with 5% nonfat dry milk, and probed with the following antibodies (Ab): caspase

3 (CST), PARP (CST), beta-Actin pAb (Invitrogen), MNV NS1/2 (a gift from Dr. Vernon Ward, U. of Otago, Australia), or MNV ProPol (a gift form Dr. Kim Green, NIH). Signal was detected using goat, anti-rabbit IgG-HRP (Jackson ImmunoResearch), developed with ECL substrate (Pierce, ThermoFisher), and imaged with an ImageQuant LAS4000 (GE Healthcare, Little Chalfont, UK).

Intestinal epithelial cell collection

Epithelial fractions were prepared by non-enzymatic striping as previously described [32]. Mice were euthanized and distal small intestine, cecum, and colon (regions of highest MNV replication) were isolated. Peyer's patches were removed from small intestine and intestinal tissues were incubated in stripping buffer (10% bovine calf serum, 15 mM HEPES, 5 mM EDTA, 5 mM dithiothreitol [DTT] in PBS) with shaking for 20 min at 37˚C. The dissociated cells were collected as the epithelial fraction, consisting predominantly of IECs and directly used for flow cytometry.

Surface and intracellular staining and flow cytometry

BV2 cells were trypsinized and washed once with 1X PBS, stained with the amine-reactive viability dye, Zombie Aqua (Biolegend, San Diego, CA) (20min, on ice), washed once with cold 2% FBS/PBS, washed once with cold Annexin V binding buffer (CST), and stained with Annexin V-FITC (CST) (15min, RT). Cells were immediately analyzed via flow cytometry on an LSR Fortessa (Becton Dickinson [BD], Franklin Lakes, NJ) with FACSDiva software (BD), and data was analyzed using FlowJo software (FlowJo LLC, Ashland, OR).

IECs isolated as described above were stained with the Zombie Aqua viability dye (Biolegend), Fc receptors were blocked with purified CD16/CD32 pAb (clone93; Biolegend), and cells were probed for surface markers, EpCAM (clone G8.8; Biolegend) and CD45 (clone 30-F11; Biolegend). Cells were subsequently fixed with 2% paraformaldehyde/PBS (10min, RT), and blocked/permeablized in 0.2% Triton X/PBS with 2% normal goat serum (20min, RT). Fixed and permeabilized cells were probed for intracellular viral antigen with 2 distinct antibodies: Rabbit polyclonal anti-NS1/2 (a gift from Dr. Vernon Ward, U. of Otago, Australia) and mouse monoclonal anti-NS1 (clone CM79, a gift from Dr. Ian Clark, U. of Southampton, UK). These unconjugated antibodies were detected with anti-Rabbit Alexa Fluor 647 (Molecular Probes, Eugene, OR), and anti-mouse Dylight 405 (Jackson ImmunoResearch), respectively. Cells were analyzed via flow cytometry, and viable cells that were EpCAM+, CD45-, NS1/2 pAb+, and NS1 mAb+ were labeled as infected epithelial cells.

RNA *in situ* hybridization via RNAscope

Ileum was opened longitudinally, pinned apical side up in wax trays, and fixed in 10% neutral-buffered formalin (Sigma) (18-24h, RT), then moved to 70% EtOH. Tissues were embedded in 2% agar (ThermoFisher), the PP was vertically transected, flipped 90 degrees, and re-embedded in 2% agar. Agar blocks were maintained in 70% EtOH prior to being paraffin-embedded. Tissue sections (5μM) were cut and maintained at RT with desiccant until processed. RNA *in situ* hybridization was performed using the RNAscope Multiplex Fluorescent v2 kit (Advanced Cell Diagnostics [ACDBio], Newark, CA) per protocol guidelines. Probes were designed by ACDBio for detection of CW3 positive strand RNA (471891-C1), CR6 positive strand RNA (502631-C1), and EpCAM mRNA (418151-C2), and signals were amplified and detected via ACDBio protocols using TSA plus technology (Perkin Elmer, Waltham, MA). Slides were mounted with ProLong Gold antifade reagent (ThermoFisher), and imaged using a Zeiss Apo-Tome2 on an Axio Imager, with a Zeiss AxioCam 506 (Zeiss, Jena, Germany).

Statistical analyses

Data were analyzed with Prism 7 software (GraphPad Prism Software, La Jolla, CA), with specified tests and significance noted in the figure legends.

Supporting information

S1 Video. M2C-CD300lf cells infected (MOI = 1) with MNV strain CW3, related to Fig 10.
(MP4)

S2 Video. M2C-CD300lf cells infected (MOI = 1) with MNV strain CR6, related to Fig 10.
(MP4)

S3 Video. M2C-CD300lf cells infected (MOI = 1) with MNV strain CR6Δcasp, related to Fig 10.
(MP4)

S4 Video. Mock-infected M2C-CD300lf cells, related to Fig 10.
(MP4)

S5 Video. M2C-CD300lf cells treated with staurosporine, related to Fig 10.
(MP4)

Acknowledgments

The authors would like to thank the OHSU Advanced Light Microscopy Core, Flow Cytometry Core, and Histopathology Shared Resource for technical support, Lena Li for overseeing mouse colonies, and Stephanie Karst for guidance with RNAscope techniques.

Author Contributions

Conceptualization: Bridget A. Robinson, Broc T. McCune, Timothy J. Nice.

Formal analysis: Bridget A. Robinson.

Funding acquisition: Timothy J. Nice.

Investigation: Bridget A. Robinson, Jacob A. Van Winkle, A. Mack Peters, Timothy J. Nice.

Methodology: Bridget A. Robinson, Jacob A. Van Winkle, Timothy J. Nice.

Project administration: Timothy J. Nice.

Resources: Broc T. McCune.

Supervision: Timothy J. Nice.

Writing – original draft: Bridget A. Robinson.

Writing – review & editing: Bridget A. Robinson, Broc T. McCune, Timothy J. Nice.

References

1. Ahmed SM, Hall AJ, Robinson AE, Verhoef L, Premkumar P, Parashar UD, et al. Global prevalence of norovirus in cases of gastroenteritis: a systematic review and meta-analysis. Lancet Infect Dis. 2014; 14: 725–730. https://doi.org/10.1016/S1473-3099(14)70767-4 PMID: 24981041
2. Glass RI, Parashar UD, Estes MK. Norovirus gastroenteritis. N Engl J Med. 2009; 361: 1776–85. https://doi.org/10.1056/NEJMra0804575 PMID: 19864676

3. Saito M, Goel-Apaza S, Espetia S, Velasquez D, Cabrera L, Loli S, et al. Multiple Norovirus Infections in a Birth Cohort in a Peruvian Periurban Community. Clin Infect Dis. 2014; 58: 483–491. https://doi.org/10.1093/cid/cit763 PMID: 24300042
4. Teunis PFM, Sukhrie FHA, Vennema H, Bogerman J, Beersma MFC, Koopmans MPG. Shedding of norovirus in symptomatic and asymptomatic infections. Epidemiol Infect. 2015; 143: 1710–7. https://doi.org/10.1017/S095026881400274X PMID: 25336060
5. Ettayebi K, Crawford SE, Murakami K, Broughman JR, Karandikar U, Tenge VR, et al. Replication of human noroviruses in stem cell-derived human enteroids. Science. 2016; 353: 1387–1393. https://doi.org/10.1126/science.aaf5211 PMID: 27562956
6. Jones MK, Watanabe M, Zhu S, Graves CL, Keyes LR, Grau KR, et al. Enteric bacteria promote human and mouse norovirus infection of B cells. Science. 2014; 346: 755–9. https://doi.org/10.1126/science.1257147 PMID: 25378626
7. Karst SM, Wobus CE. A Working Model of How Noroviruses Infect the Intestine. PLOS Pathog. 2015; 11: e1004626. https://doi.org/10.1371/journal.ppat.1004626 PMID: 25723501
8. Nice TJ, Robinson BA, Van Winkle JA. The Role of Interferon in Persistent Viral Infection: Insights from Murine Norovirus. Trends Microbiol. 2018; 26: 510–524. https://doi.org/10.1016/j.tim.2017.10.010 PMID: 29157967
9. Baldridge MT, Turula H, Wobus CE. Norovirus Regulation by Host and Microbe. Trends Mol Med. 2016; 22: 1047–1059. https://doi.org/10.1016/j.molmed.2016.10.003 PMID: 27887808
10. Karst SM, Wobus CE, Lay M, Davidson J, Virgin HW. STAT1-dependent innate immunity to a Norwalk-like virus. Science. 2003; 299: 1575–8. https://doi.org/10.1126/science.1077905 PMID: 12624267
11. Lambden PR, Caul EO, Ashley CR, Clarke IN. Sequence and genome organization of a human small round-structured (Norwalk-like) virus. Science. 1993; 259: 516–9. https://doi.org/10.1126/science.8380940 PMID: 8380940
12. Sosnovtsev S V, Belliot G, Chang K-O, Prikhodko VG, Thackray LB, Wobus CE, et al. Cleavage Map and Proteolytic Processing of the Murine Norovirus Nonstructural Polyprotein in Infected Cells. J Virol. 2006; 80: 7816–7831. https://doi.org/10.1128/JVI.00532-06 PMID: 16873239
13. Seah EL, Marshall JA, Wright PJ. trans activity of the norovirus Camberwell proteinase and cleavage of the N-terminal protein encoded by ORF1. J Virol. 2003; 77: 7150–7155. https://doi.org/10.1128/JVI.77.12.7150-7155.2003 PMID: 12768037
14. Liu B, Clarke IN, Lambden PR. Polyprotein processing in Southampton virus: identification of 3C-like protease cleavage sites by in vitro mutagenesis. J Virol. 1996; 70: 2605–10. PMID: 8642693
15. Hyde JL, Sosnovtsev S V, Green KY, Wobus C, Virgin HW, Mackenzie JM. Mouse Norovirus Replication Is Associated with Virus-Induced Vesicle Clusters Originating from Membranes Derived from the Secretory Pathway. J Virol. 2009; 83: 9709–9719. https://doi.org/10.1128/JVI.00600-09 PMID: 19587041
16. Hyde JL, Mackenzie JM. Subcellular localization of the MNV-1 ORF1 proteins and their potential roles in the formation of the MNV-1 replication complex. Virology. 2010; 406: 138–148. https://doi.org/10.1016/j.virol.2010.06.047 PMID: 20674956
17. Doerflinger SY, Cortese M, Romero-Brey I, Menne Z, Tubiana T, Schenk C, et al. Membrane alterations induced by nonstructural proteins of human norovirus. PLoS Pathog. 2017; 13: e1006705. https://doi.org/10.1371/journal.ppat.1006705 PMID: 29077760
18. Ettayebi K, Hardy ME. Norwalk Virus Nonstructural Protein p48 Forms a Complex with the SNARE Regulator VAP-A and Prevents Cell Surface Expression of Vesicular Stomatitis Virus G Protein. J Virol. 2003; 77: 11790–11797. https://doi.org/10.1128/JVI.77.21.11790-11797.2003 PMID: 14557663
19. Thorne LG, Goodfellow IG. Norovirus gene expression and replication. J Gen Virol. 2014; 95: 278–291. https://doi.org/10.1099/vir.0.059634-0 PMID: 24243731
20. Nice TJ, Strong DW, McCune BT, Pohl CS, Virgin HW. A single-amino-acid change in murine norovirus NS1/2 is sufficient for colonic tropism and persistence. J Virol. 2013; 87: 327–34. https://doi.org/10.1128/JVI.01864-12 PMID: 23077309
21. Bailey D, Thackray LB, Goodfellow IG. A Single Amino Acid Substitution in the Murine Norovirus Capsid Protein Is Sufficient for Attenuation In Vivo. J Virol. 2008; 82: 7725–7728. https://doi.org/10.1128/JVI.00237-08 PMID: 18495770
22. Strong DW, Thackray LB, Smith TJ, Virgin HW. Protruding domain of capsid protein is necessary and sufficient to determine murine norovirus replication and pathogenesis in vivo. J Virol. 2012; 86: 2950–8. https://doi.org/10.1128/JVI.07038-11 PMID: 22258242
23. Borin BN, Tang W, Nice TJ, McCune BT, Virgin HW, Krezel AM. Murine norovirus protein NS1/2 aspartate to glutamate mutation, sufficient for persistence, reorients side chain of surface exposed tryptophan

within a novel structured domain. Proteins. 2014; 82: 1200–9. https://doi.org/10.1002/prot.24484 PMID: 24273131

24. Wobus CE, Karst SM, Thackray LB, Chang K-O, Sosnovtsev S V., Belliot G, et al. Replication of Norovirus in Cell Culture Reveals a Tropism for Dendritic Cells and Macrophages. PLoS Biol. 2004; 2: e432. https://doi.org/10.1371/journal.pbio.0020432 PMID: 15562321

25. Grau KR, Roth AN, Zhu S, Hernandez A, Colliou N, DiVita BB, et al. The major targets of acute norovirus infection are immune cells in the gut-associated lymphoid tissue. Nat Microbiol. 2017; 2: 1586–1591. https://doi.org/10.1038/s41564-017-0057-7 PMID: 29109476

26. Orchard RC, Wilen CB, Doench JG, Baldridge MT, McCune BT, Lee Y-CJ, et al. Discovery of a proteinaceous cellular receptor for a norovirus. Science. 2016; 353: 933–6. https://doi.org/10.1126/science.aaf1220 PMID: 27540007

27. Haga K, Fujimoto A, Takai-Todaka R, Miki M, Doan YH, Murakami K, et al. Functional receptor molecules CD300lf and CD300ld within the CD300 family enable murine noroviruses to infect cells. Proc Natl Acad Sci U S A. 2016; 113: E6248–E6255. https://doi.org/10.1073/pnas.1605575113 PMID: 27681626

28. Wilen CB, Lee S, Hsieh LL, Orchard RC, Desai C, Hykes BL, et al. Tropism for tuft cells determines immune promotion of norovirus pathogenesis. Science. 2018; 360: 204–208. https://doi.org/10.1126/science.aar3799 PMID: 29650672

29. Lee S, Wilen CB, Orvedahl A, McCune BT, Kim K-W, Orchard RC, et al. Norovirus Cell Tropism Is Determined by Combinatorial Action of a Viral Non-structural Protein and Host Cytokine. Cell Host Microbe. 2017; 22: 449–459.e4. https://doi.org/10.1016/j.chom.2017.08.021 PMID: 28966054

30. Haber AL, Biton M, Rogel N, Herbst RH, Shekhar K, Smillie C, et al. A single-cell survey of the small intestinal epithelium. Nature. 2017; 551: 333–339. https://doi.org/10.1038/nature24489 PMID: 29144463

31. Hoffmann H-H, Schneider WM, Rice CM. Interferons and viruses: an evolutionary arms race of molecular interactions. Trends Immunol. 2015; 36: 124–38. https://doi.org/10.1016/j.it.2015.01.004 PMID: 25704559

32. Nice TJ, Osborne LC, Tomov VT, Artis D, Wherry EJJ, Virgin HW. Type I Interferon Receptor Deficiency in Dendritic Cells Facilitates Systemic Murine Norovirus Persistence Despite Enhanced Adaptive Immunity. PLoS Pathog. 2016; 12: e1005684. https://doi.org/10.1371/journal.ppat.1005684 PMID: 27327515

33. Thackray LB, Duan E, Lazear HM, Kambal A, Schreiber RD, Diamond MS, et al. Critical Role for Interferon Regulatory Factor 3 (IRF-3) and IRF-7 in Type I Interferon-Mediated Control of Murine Norovirus Replication. J Virol. 2012; 86: 13515–13523. https://doi.org/10.1128/JVI.01824-12 PMID: 23035219

34. Baldridge MT, Nice TJ, McCune BT, Yokoyama CC, Kambal A, Wheadon M, et al. Commensal microbes and interferon-λ determine persistence of enteric murine norovirus infection. Science. 2015; 347: 266–9. https://doi.org/10.1126/science.1258025 PMID: 25431490

35. Nice TJ, Baldridge MT, McCune BT, Norman JM, Lazear HM, Artyomov M, et al. Interferon-λ cures persistent murine norovirus infection in the absence of adaptive immunity. Science. 2015; 347: 269–73. https://doi.org/10.1126/science.1258100 PMID: 25431489

36. Taylor RC, Cullen SP, Martin SJ. Apoptosis: controlled demolition at the cellular level. Nat Rev Mol Cell Biol. 2008; 9: 231–41. https://doi.org/10.1038/nrm2312 PMID: 18073771

37. Polster BM, Pevsner J, Hardwick JM. Viral Bcl-2 homologs and their role in virus replication and associated diseases. Biochim Biophys Acta. 2004; 1644: 211–27. https://doi.org/10.1016/j.bbamcr.2003.11.001 PMID: 14996505

38. Galluzzi L, Brenner C, Morselli E, Touat Z, Kroemer G. Viral control of mitochondrial apoptosis. PLoS Pathog. 2008; 4: e1000018. https://doi.org/10.1371/journal.ppat.1000018 PMID: 18516228

39. Amara A, Mercer J. Viral apoptotic mimicry. Nat Rev Microbiol. 2015; 13: 461–469. https://doi.org/10.1038/nrmicro3469 PMID: 26052667

40. Richard A, Tulasne D. Caspase cleavage of viral proteins, another way for viruses to make the best of apoptosis. Cell Death Dis. 2012; 3: e277. https://doi.org/10.1038/cddis.2012.18 PMID: 22402601

41. Mebratu YA, Tipper J, Chand HS, Walton S, Harrod KS, Tesfaigzi Y. Bik Mediates Caspase-Dependent Cleavage of Viral Proteins to Promote Influenza A Virus Infection. Am J Respir Cell Mol Biol. 2016; 54: 664–73. https://doi.org/10.1165/rcmb.2015-0133OC PMID: 26437021

42. Al-Molawi N, Beardmore VA, Carter MJ, Kass GEN, Roberts LO. Caspase-mediated cleavage of the feline calicivirus capsid protein. J Gen Virol. 2003; 84: 1237–44. https://doi.org/10.1099/vir.0.18840-0 PMID: 12692289

43. Cheetham S, Souza M, Meulia T, Grimes S, Han MG, Saif LJ. Pathogenesis of a genogroup II human norovirus in gnotobiotic pigs. J Virol. 2006; 80: 10372–81. https://doi.org/10.1128/JVI.00809-06 PMID: 17041218

44. Troeger H, Loddenkemper C, Schneider T, Schreier E, Epple H-J, Zeitz M, et al. Structural and functional changes of the duodenum in human norovirus infection. Gut. 2009; 58: 1070–7. https://doi.org/10.1136/gut.2008.160150 PMID: 19036950

45. Mumphrey SM, Changotra H, Moore TN, Heimann-Nichols ER, Wobus CE, Reilly MJ, et al. Murine norovirus 1 infection is associated with histopathological changes in immunocompetent hosts, but clinical disease is prevented by STAT1-dependent interferon responses. J Virol. 2007; 81: 3251–3263. https://doi.org/10.1128/JVI.02096-06 PMID: 17229692

46. Bok K, Prikhodko VG, Green KY, Sosnovtsev S V. Apoptosis in Murine Norovirus-Infected RAW264.7 Cells Is Associated with Downregulation of Survivin. J Virol. 2009; 83: 3647–3656. https://doi.org/10.1128/JVI.02028-08 PMID: 19211757

47. Furman LM, Maaty WS, Petersen LK, Ettayebi K, Hardy ME, Bothner B. Cysteine protease activation and apoptosis in Murine norovirus infection. Virol J. 2009; 6: 139. https://doi.org/10.1186/1743-422X-6-139 PMID: 19744337

48. Herod MR, Salim O, Skilton RJ, Prince CA, Ward VK, Lambden PR, et al. Expression of the Murine Norovirus (MNV) ORF1 Polyprotein Is Sufficient to Induce Apoptosis in a Virus-Free Cell Model. PLoS One. 2014; 9: e90679. https://doi.org/10.1371/journal.pone.0090679 PMID: 24599381

49. Van Winkle JA, Robinson BA, Peters AM, Li L, Nouboussi R V, Mack M, et al. Persistence of Systemic Murine Norovirus Is Maintained by Inflammatory Recruitment of Susceptible Myeloid Cells. Cell Host Microbe. 2018; 24: 665–676.e4. https://doi.org/10.1016/j.chom.2018.10.003 PMID: 30392829

50. Lee S, Liu H, Wilen CB, Sychev ZE, Desai C, Hykes BL, et al. A Secreted Viral Nonstructural Protein Determines Intestinal Norovirus Pathogenesis. Cell Host Microbe. 2019; 25: 845–857.e5. https://doi.org/10.1016/j.chom.2019.04.005 PMID: 31130511

51. Chang HY, Yang X. Proteases for cell suicide: functions and regulation of caspases. Microbiol Mol Biol Rev. 2000; 64: 821–46. https://doi.org/10.1128/mmbr.64.4.821-846.2000 PMID: 11104820

52. McCune BT, Tang W, Lu J, Eaglesham JB, Thorne L, Mayer AE, et al. Noroviruses Co-opt the Function of Host Proteins VAPA and VAPB for Replication via a Phenylalanine-Phenylalanine-Acidic-Tract-Motif Mimic in Nonstructural Viral Protein NS1/2. MBio. 2017; 8: 1–17. https://doi.org/10.1128/mBio.00668-17 PMID: 28698274

53. Feng Z, Hensley L, McKnight KL, Hu F, Madden V, Ping L, et al. A pathogenic picornavirus acquires an envelope by hijacking cellular membranes. Nature. 2013; 496: 367–71. https://doi.org/10.1038/nature12029 PMID: 23542590

54. Chen Y-H, Du W, Hagemeijer MC, Takvorian PM, Pau C, Cali A, et al. Phosphatidylserine Vesicles Enable Efficient En Bloc Transmission of Enteroviruses. Cell. 2015; 160: 619–630. https://doi.org/10.1016/j.cell.2015.01.032 PMID: 25679758

55. Bhattacharyya S, Zagórska A, Lew ED, Shrestha B, Rothlin C V, Naughton J, et al. Enveloped viruses disable innate immune responses in dendritic cells by direct activation of TAM receptors. Cell Host Microbe. 2013; 14: 136–47. https://doi.org/10.1016/j.chom.2013.07.005 PMID: 23954153

56. Santiana M, Ghosh S, Ho BA, Rajasekaran V, Du WL, Mutsafi Y, et al. Vesicle-Cloaked Virus Clusters Are Optimal Units for Inter-organismal Viral Transmission. Cell Host Microbe. 2018; 208–220. https://doi.org/10.1016/j.chom.2018.07.006 PMID: 30092198

57. Gerbe F, Sidot E, Smyth DJ, Ohmoto M, Matsumoto I, Dardalhon V, et al. Intestinal epithelial tuft cells initiate type 2 mucosal immunity to helminth parasites. Nature. 2016; 529: 226. https://doi.org/10.1038/nature16527 PMID: 26762460

58. Von Moltke J, Ji M, Liang HE, Locksley RM. Tuft-cell-derived IL-25 regulates an intestinal ILC2-epithelial response circuit. Nature. 2016; 529: 221–225. https://doi.org/10.1038/nature16161 PMID: 26675736

59. Delgado ME, Grabinger T, Brunner T. Cell death at the intestinal epithelial front line. FEBS J. 2016; 283: 2701–19. https://doi.org/10.1111/febs.13575 PMID: 26499289

60. Reginato MJ, Mills KR, Paulus JK, Lynch DK, Sgroi DC, Debnath J, et al. Integrins and EGFR coordinately regulate the pro-apoptotic protein Bim to prevent anoikis. Nat Cell Biol. 2003; 5: 733–40. https://doi.org/10.1038/ncb1026 PMID: 12844146

61. Hausmann M, Leucht K, Ploner C, Kiessling S, Villunger A, Becker H, et al. BCL-2 modifying factor (BMF) is a central regulator of anoikis in human intestinal epithelial cells. J Biol Chem. 2011; 286: 26533–40. https://doi.org/10.1074/jbc.M111.265322 PMID: 21673109

62. Youle RJ, Strasser A. The BCL-2 protein family: opposing activities that mediate cell death. Nat Rev Mol Cell Biol. 2008; 9: 47–59. https://doi.org/10.1038/nrm2308 PMID: 18097445

63. Poon IKH, Lucas CD, Rossi AG, Ravichandran KS. Apoptotic cell clearance: basic biology and therapeutic potential. Nat Rev Immunol. 2014; 14: 166–180. https://doi.org/10.1038/nri3607 PMID: 24481336

64. Lee CS, Penberthy KK, Wheeler KM, Juncadella IJ, Vandenabeele P, Lysiak JJ, et al. Boosting Apoptotic Cell Clearance by Colonic Epithelial Cells Attenuates Inflammation In Vivo. Immunity. 2016; 44: 807–20. https://doi.org/10.1016/j.immuni.2016.02.005 PMID: 27037190

65. Juncadella IJ, Kadl A, Sharma AK, Shim YM, Hochreiter-Hufford A, Borish L, et al. Apoptotic cell clearance by bronchial epithelial cells critically influences airway inflammation. Nature. 2013; 493: 547–51. https://doi.org/10.1038/nature11714 PMID: 23235830

66. Monks J, Rosner D, Geske FJ, Lehman L, Hanson L, Neville MC, et al. Epithelial cells as phagocytes: apoptotic epithelial cells are engulfed by mammary alveolar epithelial cells and repress inflammatory mediator release. Cell Death Differ. 2005; 12: 107–14. https://doi.org/10.1038/sj.cdd.4401517 PMID: 15647754

67. Blasi E, Barluzzi R, Bocchini V, Mazzolla R, Bistoni F. Immortalization of murine microglial cells by a v-raf/v-myc carrying retrovirus. J Neuroimmunol. 1990; 27: 229–37. https://doi.org/10.1016/0165-5728(90)90073-V PMID: 2110186

68. Qin Z, Noffz G, Mohaupt M, Blankenstein T. Interleukin-10 prevents dendritic cell accumulation and vaccination with granulocyte-macrophage colony-stimulating factor gene-modified tumor cells. J Immunol. 1997; 159: 770–6. PMID: 9218594

69. Gonzalez-Hernandez MB, Liu T, Payne HC, Stencel-Baerenwald JE, Ikizler M, Yagita H, et al. Efficient Norovirus and Reovirus Replication in the Mouse Intestine Requires Microfold (M) Cells. J Virol. 2014; 88: 6934–6943. https://doi.org/10.1128/JVI.00204-14 PMID: 24696493